Article

Multi-Response Design Optimisation of a Combined Fluidised Bed-Infrared Dryer for Terebinth (*Pistacia atlantica* L.) Fruit Drying Process Based on Energy and Exergy Assessments by Applying RSM-CCD Modelling

Iman Golpour [1,*], Mohammad Kaveh [2], Ana M. Blanco-Marigorta [3], José Daniel Marcos [4], Raquel P. F. Guiné [5,*], Reza Amiri Chayjan [6], Esmail Khalife [7] and Hamed Karami [8]

[1] Department of Mechanical Engineering of Biosystems, Urmia University, Urmia 57561-51818, Iran
[2] Department of Petroleum Engineering, College of Engineering, Knowledge University, Erbil 44001, Iraq
[3] Department of Process Engineering, University of Las Palmas de Gran Canaria, 35017 Las Palmas de Gran Canaria, Spain
[4] Department of Energy Engineering, National Distance Education University, UNED, 28040 Madrid, Spain
[5] CERNAS Research Centre, Department of Food Industry, Polytechnic Institute of Viseu, 3504-510 Viseu, Portugal
[6] Department of Biosystems Engineering, Faculty of Agriculture, Bu-Ali Sina University, Hamedan 65178-33131, Iran
[7] Department of Civil Engineering, Cihan University-Erbil, Kurdistan Region, Erbil 44001, Iraq
[8] Department of Biosystems Engineering, University of Mohaghegh Ardabili, Ardabil 56199-11367, Iran
* Correspondence: imangolpour@gmail.com (I.G.); raquelguine@esav.ipv.pt (R.P.F.G.)

Abstract: The present investigation aimed to perform an optimisation process of the thermodynamic characteristics for terebinth fruit drying under different drying conditions in a fluidised bed-infrared (FBI) dryer using response surface methodology (RSM) based on a central composite design (CCD) approach. The experiments were conducted at three levels of drying air temperature (40, 55, and 70 °C), three levels of drying air velocity (0.93, 1.765, and 2.60 m/s), and three levels of infrared power (500, 1000, and 1500 W). Energy and exergy assessments of the thermodynamic parameters were performed based on the afirst and second laws of thermodynamics. Minimum energy utilisation, energy utilisation ratio, and exergy loss rate, and maximum exergy efficiency, improvement potential rate, and sustainability index were selected as the criteria in the optimisation process. The considered surfaces were evaluated at 20 experimental points. The experimental results were evaluated using a second-order polynomial model where an ANOVA test was applied to identify model ability and optimal operating drying conditions. The results of the ANOVA test showed that all of the operating variables had a highly significant effect on the corresponding responses. At the optimal drying conditions of 40 °C drying air temperature, 2.60 m/s air velocity, 633.54 W infrared power, and desirability of 0.670, the optimised values of energy utilisation, energy utilisation ratio, exergy efficiency, exergy loss rate, improvement potential rate, and sustainability index were 0.036 kJ/s, 0.029, 86.63%, 0.029 kJ/s, 1.79 kJ/s, and 7.36, respectively. The models predicted for all of the responses had R^2-values ranging between 0.9254 and 0.9928, which showed that they had good ability to predict these responses. Therefore, the results of this research showed that RSM modelling had acceptable success in optimising thermodynamic performance in addition to achieving the best experimental conditions.

Keywords: terebinth; hybrid fluidised bed infrared drying; exergy assessment; optimisation; response surface methodology (RSM)

1. Introduction

Terebinth (*Pistacia atlantica*) is a specific fruit with a sour taste, a spherical shape, and a dark green colour, which is extensively grown in the cold regions of Iran, particularly in

provinces such as Kurdistan, West Azerbaijan, Ilam, and Kermanshah, and it is also grown in other countries, including Armenia, Turkey, Syria, and Iraq [1,2]. This particular fruit not only contains a rich source of vitamins (A, B, and D), carbohydrates, protein, minerals, and nutrients, but is also rich in flavonoid compounds, anthocyanin, fatty acids, total phenolic content, and fundamental oils, which can be applied in medicine to treat cancer and inflammatory bowel disease, to strengthen the nerves, to prevent osteoporosis and anaemia, and to treat chapped lips. Besides, it can be used in the mineral, chemical, and wood processing industries [3,4]. To prevent microbial spoilage and the diverse physical, chemical, and nutritional alterations in fresh agricultural crops after harvesting, due to their high moisture content, different ways and technologies are utilised to extend their shelf life while also preserving their quality for usage and for chemical, physical, and microbiological applications [5–7].

Preservation methods, such as the drying process, are commonly used to reduce moisture content, which reduces the volume and mass parameters of food products to help decrease the prices of packaging process, storage stage, and transportation system [6,8]. Some technologies of drying systems in the food industries, including hot-air convection, microwave, infrared radiation, vacuum drying, freezing, and solar drying, have been utilised to dry agricultural crops [9–11]. Convective drying is known as the earliest way of removing moisture from foods and fresh agricultural products, such as fruits and vegetables. Various parameters, including thermophysical characteristics, air temperature, air velocity, and relative humidity, can affect the drying process when convective dryers are used in the food industries [8,12].

One of the most important advantages of applying a fluidised bed dryer (FBD), among all convective dryers, is the uniform drying of agricultural products. Still, this technique requires a large drying time because of the lower drying rate [13]. This kind of dryer, among different industrial or commercial dryers, also has specific disadvantages, including low efficiency, long time of drying process, great rate of energy consumption, and reduced final quality of products. This leads to the use of other types of equipment for drying agricultural products [14,15]. These issues could be majorly resolved by using hybrid dryers with a combination of infrared radiation and convective drying methods to obtain dried fruits and vegetables with high final quality. Infrared radiation (IR) drying is used as one of the most potent techniques for drying products with great moisture content (MC). This process involves the transfer of IR energy straight from an IR lamp as the energy source to the product surface without influencing the air temperature around the samples [16,17]. The use of hybrid IR-convective dryers in the food industries has advantages, such as saving drying time, rapid transient response, great coefficient of heat transfer, and especially short energy consumption and high energy efficiency, and can resolve the problems related to convective dryers to produce final dried products with better quality for consumption [16,18].

Although the use of energy assessment based on the first law of thermodynamics in energy facilities, including industrial drying systems, is important, it does not provide any information regarding the energy quality and locations of improvement because of irreversibility, exergy losses, and surrounding conditions in the related processing system. In addition, it could not be used for optimisation aims and sustainable design in the food industries [19,20]. From the viewpoint of the second law of thermodynamics, exergy analysis as a maximum work obtained in a system can overcome the aforementioned shortcomings; thus, it is extensively utilised as a required instrument for surmounting the deficiency of energy analysis, improving energy systems, designing suitable process and operation procedures, analysing and optimising heating systems, as well as enabling the identification of the locations, kinds, and real magnitudes of energy and exergy losses [20–24]. Several investigations have been conducted based on the energy and exergy assessments of a forced convection cabinet dryer for the drying process of okra [9], a convective dryer for paddy drying [22], a fluidised dryer for drying eggplant [25], a microwave dryer for mulberry

drying [26], a multi-stage, semi-industrial continuous dryer for onion drying [27], and an infrared-convective dryer for walnut drying [28].

In recent decades, not only the prices of energy, global warming, and world population are increasing, but also fossil fuel recourses are decreasing over the world. This makes the optimal use of energy in heating systems, such as diverse dryers, of particular importance [21]. The optimisation process of energetic and exergetic parameters is regularly conducted in the food industries to resolve ongoing problems and related challenges in energy systems to improve efficiencies and increase the quality of the final products, or to optimise the cost factor of the production process [29]. Response surface methodology (RSM) as a statistical–mathematical method is employed to predict and optimise multivariate statistical modelling equations in multiple regression analyses and optimisation investigations. RSM helps experimenters and designers make efficient identification of a process or system through the application of quantitative data acquired from accurately designed experiments [30]. Benhamza et al. [31] conducted an optimisation process of the exergy parameters of a solar air heater for food drying using RSM. They concluded that the optimal outlet temperature, $I\dot{P}$, and thermal efficiency were 52 °C, 1397.34 W, and 51.78%, respectively. The optimal design improved the $I\dot{P}$ by 19.33% and thermal efficiency by 15.76%. Majdi et al. [8] applied RSM to optimise the convective drying of apple slices, and the maximum value of the desirability function was reported to be 0.781 to obtain optimal conditions and responses.

Although there are several studies on the energy and exergy assessments of several systems for drying agricultural crops, a literature review shows no sufficient information regarding the optimisation of thermodynamic properties of terebinth fruit drying in a hybrid fluidised bed-infrared dryer by applying CCD-RSM. As a consequence, the main aims of this study were to develop a predictive RSM optimisation model to forecast the optimal drying conditions for terebinth drying in a hybrid fluidised bed-infrared dryer, as well as to apply a comprehensive exergy analytical technique to the energetic and exergetic parameters under investigation, including energy utilisation (EU), energy utilisation ratio (EUR), exergetic efficiency, exergetic loss rate, improvement potential rate, and sustainability index.

2. Materials and Methods

2.1. Terebinth Samples

Fresh samples of terebinth fruit were harvested from the local forests located in the city of Sardasht, West Azerbaijan, Iran. After manually washing, cleaning, and removing defective fruits and foreign particles, the terebinth samples prepared for the experiments were kept in a polyethylene plastic to maintain their original quality in a refrigerator at 4 ± 1 °C. The average primary moisture content (MC) of the fresh terebinth samples was obtained at 1.16 ± 0.5% (d.b.%) using a standard oven method (Memmert, UFB 500, Schwabach, Germany) at 70 ± 2 °C for 24 h [2].

2.2. Equipment Description and Experimental Configuration

A schematic of the experimental setup of a laboratory-scale hybrid fluidised bed-infrared (FBI) dryer that was used to conduct the drying experiments is shown in Figure 1. The main parts of the FBI dryer consisted of an electrical air heating chamber (2.4 kW), an adjustable centrifugal blower, a drying chamber, four infrared lamps (Philips, Belgium) with 2000 W power, a thermostat (Atbin, Mega, Tehran, Iran), an inverter (LS, Seoul, Republic of Korea), and a tray sample. The FBI dryer was fixed for 30 min before starting each drying experiment to reach stable conditions. To equilibrate the sample temperature with the ambient temperature, a certain amount of the terebinth samples was taken out of the refrigerator one hour before starting the drying experiments. A total of 40 g of the fresh terebinth samples (1.16% M.C.) was utilised to conduct the drying experiments at three levels of air temperature (40, 55, and 70 °C), three levels of drying air velocity (0.93, 1.76, and 2.60 m/s), and three levels of infrared power (500, 1000, and 1500 W) in the FBI

dryer. The value of relative humidity was found to be in the range of 24–29%. The terebinth samples were weighed during the FBI drying process using a digital balance (AND GF6000, Tokyo, Japan) with an accuracy of 0.01 g. The drying experiments of the terebinth samples were performed in three replications.
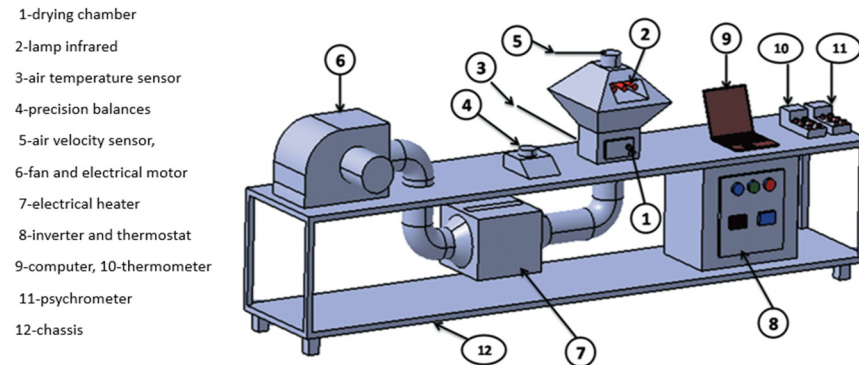

1-drying chamber
2-lamp infrared
3-air temperature sensor
4-precision balances
5-air velocity sensor,
6-fan and electrical motor
7-electrical heater
8-inverter and thermostat
9-computer, 10-thermometer
11-psychrometer
12-chassis

Figure 1. A schematic of the hybrid fluidised bed-infrared dryer.

2.3. Comprehensive Energy and Exergy Analyses

In this study, the conservation principles of mass and energy and the general equation of exergy balance were utilised for a comprehensive exergy assessment to analyse the exergy rate of streams under the process of general steady flow in the hybrid infrared drying system. Table 1 demonstrates the general equations utilised to calculate the performance parameters as well as the inflow, outflow, and exergy loss rate.

Table 1. General equations applied to calculate the relevant parameters in conventional energy and exergy analyses [32].

Parameter	Equation	Equation No.
Mass balance	$\sum \dot{m}_{in} = \sum \dot{m}_{out}$	(1)
Energy balance	$\sum \dot{En}_{in} = \sum \dot{En}_{out}$	(2)
Exergy balance	$(\dot{Ex}^{ph}_{Tein} + \dot{Ex}_{a,in} + \dot{Ex}_{IR}) - (\dot{Ex}^{ph}_{Teout} \dot{Ex}_{a,out} + \dot{Ex}_{eva}) = \sum \dot{Ex}_{Loss}$	(3)

Energy utilisation, EU, was obtained with respect to the principle of energy conservation using the following formula [33]:

$$EU = \dot{m}_{da}(h_{dcin} - h_{dcout}) + \dot{m}_{te}(h_{tein} - h_{teout}) \tag{4}$$

The energy utilisation ratio (EUR) of the hybrid infrared dryer was computed as follows [34]:

$$EUR = \frac{\dot{m}_{da}(h_{dcin} - h_{dcout}) + \dot{m}_{te}(h_{tein} - h_{teout})}{\dot{m}_{da}c_{Pda}(T_{tein} - T_{teout})} \tag{5}$$

The enthalpy of drying air (h_{da}) and the enthalpy of the terebinth samples (h_{te}) were determined using Equation (6) [35] and Equation (7) [33]:

$$h_{da} = c_{pa}(T - T_0) + \omega h_{fg} \tag{6}$$

$$h_{te} = c_{Pte}(T_{te} - T_0) \tag{7}$$

The average specific heat of drying air (c_{pa}) and the specific heat of fresh and dried terebinth (c_{te}) were obtained using Equation (8) [35] and Equation (9) [36]:

$$c_{pa} = 1.004 + 1.88\omega \tag{8}$$

$$c_{te} = 4.187X_m + 1.424X_c + 1.459X_{pr} + 1.675X_f + 0.837X_a \tag{9}$$

The exergy rate of air inlet and outlet of the drying chamber were obtained using the following Equation [19,37]:

$$\dot{Ex}_{da} = \dot{m}_{da}\left\{(c_a + \omega c_v)(T_a - T_0) - T_0\left[(c_a + \omega c_v)\ln\left(\frac{T}{T_0}\right)\right] - (R_a + \omega R_v)\ln\left(\frac{P_a}{P_0}\right)\right\} + \dot{m}_{da}\left\{T_0\left[(R_a + \omega R_v)\ln\left(\frac{1+1.6078\omega_0}{1+1.6078\omega}\right)\right] + 1.6078\omega R_a\ln\left(\frac{\omega}{\omega_0}\right)\right\}$$ (10)

The mass flow rate of drying air was obtained using Equation (11) [34]:

$$\dot{m}_a = \rho_a u_a A_a$$ (11)

In Equation (10), the humidity ratio of air (ω_a) is calculated using Equation (12) [38]:

$$\omega = 0.622\frac{\varphi P_{vs,a}}{P_{da} - \varphi P_{vs,a}}$$ (12)

The exergy input rate of the IR source was calculated using the following Equation [19,39]:

$$\dot{Ex}_{IR} = \left(T_{IR}^4 - \frac{4}{3}T_{IR}^3 T_0 + \frac{1}{3}T_0^4\right) \times \varepsilon_{IR} \times \sigma \times A_{IR}$$ (13)

The rate of exergy transfer for the evaporation section of the FBI dryer was defined using the following Equation [40]:

$$\dot{Ex}_{evp} = \left(1 - \frac{T_\infty}{T_a}\right)\dot{m}_a h_{fg}$$ (14)

The latent heat of vaporisation of moisture on the basis of absolute temperature was determined at saturation state using the Equation below [41]:

$$h_{fg} = \begin{cases} 2.503 \times 10^6 - 2.386 \times 10^3(T - 273.16) & 273.16 \leq T(K) \leq 338.72 \\ (7.33 \times 10^{12} - 1.60 \times 10^7 T^2)^{\frac{1}{2}} & 338.72 \leq T(K) \leq 533.16 \end{cases}$$ (15)

The exergy rate of the wet terebinth samples could be identified using the following formula [42]:

$$\dot{Ex}_{te}^{ph} = \dot{m}_{te} c_{pte}\left[(T_{te} - T_\infty) - T_\infty\ln\left(\frac{T_{te}}{T_\infty}\right)\right]$$ (16)

The exergetic efficiency of the drying chamber (ψ_{ex}) was computed using Equation (17) [9]:

$$Ex_{eff} = (1 - \frac{\dot{Ex}_{loss}}{\dot{Ex}_{in}}) \times 100$$ (17)

The improvement potential rate ($\dot{IP}$) was obtained as follows [43]:

$$\dot{IP} = \left(1 - Ex_{eff}\right)\left(\dot{Ex}_{in} - \dot{Ex}_{out}\right)$$ (18)

Moreover, the sustainability index (*SI*) was computed using the following formula [9]:

$$SI = \frac{1}{1 - Ex_{eff}}$$ (19)

Some assumptions were made in the analysis, including the following:

1. The system of the drying process and related main components were supposed to run in steady-state conditions.
2. Kinetic and potential energies were considered negligible during the process.
3. The temperature gradient available inside the terebinth samples was considered negligible.

4. The temperature and the relative humidity of the ambient air during the drying experiments were assumed to be constant.
5. The reference state temperature and pressure were 20 °C and 101.325 kPa, respectively.
6. The change in the pressure of the inlet and outlet flows of the FBI dryer was considered negligible.
7. There was no reaction in the calculation of mass balance.

2.4. Uncertainty Analysis

Uncertainty analyses of the results of the drying experiments in this research work were divided into two special categories, namely uncertainty in the direct measurement of the independent factors and uncertainty in the results obtained from multiple factors. The first category of related uncertainties was evaluated by iterating each drying experiment at least three times and computing their standard deviation. The second category for the results obtained from multiple factors was assessed using the Taylor series method for propagation of uncertainties. Each test was performed at least three times and the maximum uncertainty of the independent factors was computed. For the dependent factors, the maximum propagated uncertainties were approximated using the Tree Calculator Release 0.9.9 software. The accuracy of the drying experiments could be obtained by applying the measurements of uncertainty using the following formula [44]:

$$U_F = \left[\left(\frac{\partial F}{\partial z_1} u_1 \right)^2 + \left(\frac{\partial F}{\partial z_2} u_2 \right)^2 + \ldots + \left(\frac{\partial F}{\partial z_n} u_n \right)^2 \right]^{1/2} \tag{20}$$

2.5. RSM Modelling

2.5.1. Multivariate Design of Experiment

In this study, a central composite experimental design (CCD) with five central points in standard RSM was applied to model the response surface and to optimise the hybrid infrared dryer during the drying of terebinth fruit. The operating ranges, the different levels of the independent factors used in this study, and the related responses of the hybrid fluidised bed-infrared dryer (FBI) experiments are presented in Table 2. The analysis applied the parameters of the drying process coded to compare the relative significance of factors and to identify the independent factors. In this investigation, as shown in Table 3, on the basis of the face-centered CCD with RSM modelling, a total of 20 runs were accomplished with three independent factors, namely drying air temperature, air velocity, and infrared power. The relevant responses were energy utilisation, energy utilisation ratio, exergetic efficiency, exergetic loss rate, improvement potential rate, and sustainability index (Table 3). An analysis of variance (ANOVA) was employed to assess model adequacy and to identify coefficients of regression and statistical significance. Statistical assessment was also performed using RSM in the Design–Expert software (Version 13.0.0., Trial) (Stat-Ease, Minneapolis, MN, USA). The relevant results for the independent variables were statistically evaluated at the significance level of 95% (p = 0.05). The model adequacy was appraised using determination coefficient (R^2), model p-value, and lack of fit testing. Moreover, the prediction accuracy of the relevant response factors was examined using diagnostic plots, including the plots of the normal probability, the plots of the residual response factors, the plots of externally studentised residuals against the run number, and determination coefficient (R^2). In addition, the adequacies of the models were examined using adjusted-R^2, predicted R^2, and variation coefficient (CV). It should be noted that the reliability and validity of the models in predicting the experimental data were considered as a function of the Lambda value for each response factor. The flowchart and procedure of the response surface method employed to optimise the energetic and exergetic parameters in the hybrid fluidised-bed infrared dryer are shown in Figure 2.

Table 2. Experimental layout of the independent factors, related levels, criteria, and goals of the randomised polynomial treatment design for the numerical optimisation process.

			Symbol			Range and Levels		
	Parameters	Units	Uncoded	Coded	Targets	Coded	Actual	Importance
Input parameters	Infrared power	W	P	A	In range	−1 0 1	500 1000 1500	3
	Air temperature	°C	T	B	In range	−1 0 1	40 55 70	3
	Air velocity	m/s	V	C	In range	−1 0 1	0.93 1.76 2.60	3
Responses	Energy utilisation	kJ/s	EU		Minimum		0.021–0.143	3
	Energy utilisation ratio	-	EUR		Minimum		0.173–0.553	3
	Exergy loss rate	kJ/s	Ex_{loss}		Minimum		0.010–0.100	3
	Exergy efficiency	%	Ex_{eff}		Maximum		50.58–87.57	3
	Exergetic improvement potential rate	kJ/s	$\dot{IP}$		Maximum		0.64–6.65	3
	Sustainability index	-	SI		Maximum		2.02–8.05	3

Table 3. Experimental central composite design (CCD) of the input and response factors for drying terebinth under different hybrid fluidised bed-infrared drying conditions.

	Input Variables			Output Responses					
Run	T °C	V m/s	P W	EU kJ/s	EUR -	Ex_{loss} kJ/s	Ex_{eff} %	$\dot{IP}$ kJ/s	SI -
1	40	0.93	1500	0.059	0.259	0.031	74.00	3.01	3.85
2	55	1.765	1500	0.109	0.432	0.067	63.91	4.24	2.77
3	70	2.6	1500	0.143	0.553	0.100	60.39	6.65	2.52
4	55	1.765	500	0.063	0.324	0.032	73.82	2.46	3.82
5	55	1.765	1000	0.093	0.420	0.053	67.71	3.47	3.10
6	55	2.6	1000	0.100	0.450	0.065	72.96	4.28	3.70
7	40	2.6	1500	0.093	0.361	0.065	81.12	4.41	5.30
8	55	1.765	1000	0.093	0.420	0.053	67.71	3.47	3.10
9	70	2.6	500	0.085	0.421	0.047	74.23	4.87	3.88
10	55	1.765	1000	0.093	0.420	0.053	67.71	3.47	3.10
11	70	0.93	1500	0.120	0.454	0.072	50.58	3.98	2.02
12	40	2.6	500	0.026	0.234	0.019	87.57	1.50	8.05
13	55	1.765	1000	0.093	0.420	0.053	67.71	3.47	3.10
14	55	0.93	1000	0.083	0.376	0.039	65.52	2.90	2.90
15	55	1.765	1000	0.093	0.420	0.053	67.71	3.47	3.10
16	40	1.765	1000	0.033	0.240	0.020	80.06	2.08	5.02
17	70	0.93	500	0.068	0.380	0.027	62.43	2.90	2.66
18	40	0.93	500	0.021	0.173	0.010	79.05	0.64	4.77
19	55	1.765	1000	0.093	0.420	0.053	67.71	3.47	3.10
20	70	1.765	1000	0.110	0.446	0.068	64.02	4.76	2.78

Twenty experimental points of the CCD were defined to attain the relevant responses under various combinations of the three variables, as shown in Table 3.

A second-order polynomial model was fitted to the experimental data and evaluated using the Design–Expert statistical software package. The general formula for a second-degree polynomial model with three independent factors is as follows [45]:

$$Y = \alpha_0 + \sum_{i=1}^{k} \alpha_i x_i + \sum_{i=1}^{k} \alpha_{ii} x_i^2 + \sum_{i=1}^{k-1} \sum_{j=1}^{k} \alpha_{ij} x_i x_j + \delta \tag{21}$$

In the next step, five second-order polynomial equations were fitted to the experimental data based on the least-squares optimisation approach. The 3-D response surface plots were drawn using the function of two factors while keeping the others constant, and were applied in the prediction of the results.

A numerical assessment of the optimisation process of the independent factors according to multiple responses, with the desired goals to maximise exergy efficiency, exergetic improvement potential rate, and sustainability index and to minimise energy utilisation, energy utilisation ratio, and exergy loss rate, were conducted. Additionally, a desirability function (D_x) as an overall composite function was estimated for the optimisation process of multiple responses to select the optimal conditions using Equation (22) [8]:

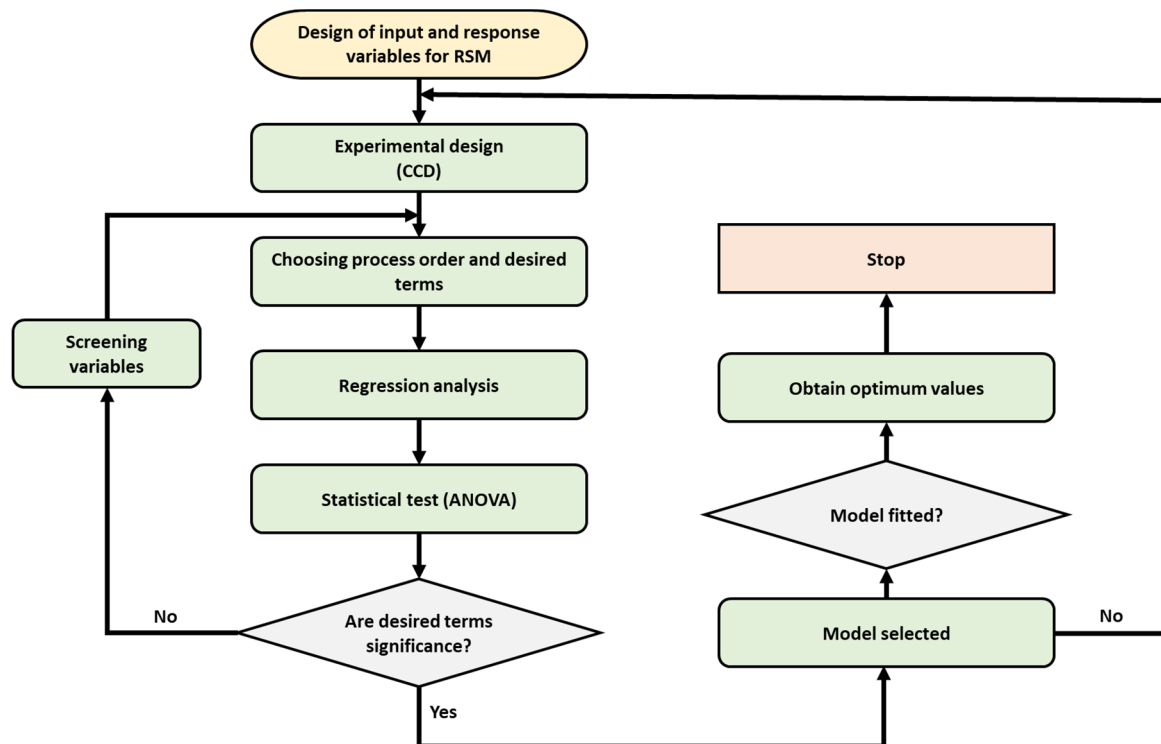$$D(x) = (Y_1 \times Y_2 \times \ldots \times Y_i)^{\frac{1}{n}} \tag{22}$$

Figure 2. The flowchart of the RSM used in the hybrid fluidised bed-infrared drying process.

2.5.2. Model Performance Evaluation

In this study, the coefficient of determination (R^2), the adjusted coefficient of determination (R^2), and the prediction error sum of squares (PRESS) were used to evaluate the experimental data and related results to predict the drying process [46]. The obtained values of R^2 and R^2_{Adj} are the indicators of how well a model of regression fits the observation data. Moreover, the values of PRESS and pred R^2 are considered the indicators of how well a model of regression predicts new observations.

$$R^2 = 1 - \frac{SS_{residual}}{SS_{total}} \tag{23}$$

$$R^2_{Adj} = 1 - \frac{SS_{residual} / DF_{residual}}{SS_{total} / DF_{total}} \tag{24}$$

$$PRESS = \sum_1^n (y_i - \overline{y}_i)^2 \tag{25}$$

$$R^2_{pred} = 1 - \frac{PRESS}{SS_{total}} \tag{26}$$

3. Results and Discussion

In this study, the impacts of the independent factors, consisting of drying air temperature, air velocity, and infrared power, in a hybrid fluidised bed-infrared dryer, on the responses, namely energy utilisation (EU), energy utilisation ratio (EUR), exergetic efficiency, exergy loss rate, exergetic improvement potential rate, and sustainability index, were investigated. The optimal values of these parameters were determined using CCD-RSM modelling. An ANOVA test was performed to analyse the model fitness and identify significant impacts of the independent variables on the responses, and to fit the second-order polynomial models to the obtained experimental data.

3.1. Experimental Uncertainty

An analysis of uncertainty was performed on the experimental measurements of relevant factors and the desired overall uncertainties of the predicted values resulting from measurement errors to confirm the repeatability and reliability of the experimental data. The results related to the analysis of uncertainty are presented in Table 4. Values of uncertainty that are less than 5% are commonly considered admissible to replicate an experiment [40,42].

Table 4. Uncertainties of the measured parameters and overall uncertainties of predicted values during the drying of terebinth in the fluidised bed-infrared dryer.

Parameter	Unit	Uncertainty (%)
Experimental measurements		
Inlet–outlet air temperature in fluidised bed-infrared dryer	°C	±0.22
Ambient air temperature	°C	±0.22
Drying cabinet inlet temperature	°C	±0.22
Drying cabinet outlet temperature	°C	±0.22
Weight loss of dried product	g	±0.401
Relative humidity of drying air	RH	±0.80
Drying air velocity	m/s	±0.05
Calculated parameters		
Uncertainty in energy utilisation ratio (EUR)	−	±0.0005
Uncertainty in energy utilisation	kJ/s	±0.004
Uncertainty in exergy loss rate	kJ/s	±0.0004
Uncertainty in exergy efficiency	%	±1.23
Uncertainty in exergetic potential improvement rate	kJ/s	0.20
Uncertainty in sustainability index	−	0.05

3.2. Evaluation of EU and EUR

3.2.1. The Model Analysis and Assessment for EU and EUR

Table 5 presents the results of the ANOVA test of the response surface quadratic models for the responses of energy utilisation and energy utilisation ratio. The ANOVA results for the RSM quadratic model of energy utilisation (EU) identified an F-value of 48.31, p-value < 0.0001, and a coefficient of variation (CV) = 7.64%, showing that the quadratic model to predict this parameter was highly significant and the drying experiments were extremely accurate and reputable (Table 5). The great Fisher's "F" value depicts whether the application of a regression equation can predict most of the related changes in the responses, while the probability value is applied to determine if F is great enough to illustrate statistical meaning. The model is statistically significant if p-value is less than 0.05 [29]. The significance of the regression model for the response of EUR was apparent from the approximated Fisher's "F" value of 106.93 and a value of probability (P) lower than 0.0001, with a CV value of 3.37%. The results showed that the model was fitted to the experimental data, as illustrated in Table 5 (p < 0.01).The reliability of an experiment commonly declines as the coefficient of variation (CV) becomes greater [45]. Both two responses (EU and EUR) showed low values of CV (<10), which showed the high relia-

bility of the experiments. These results were in agreement with the results reported by Soltani et al. [45].

Table 5. ANOVA results of the quadratic model factors of the RSM on the responses of energy utilisation and energy utilisation ratio.

	EU				EUR			
Source	**SS**	**MS**	**F-Value**	***p*-Value**	**SS**	**MS**	**F-Value**	***p*-Value**
Model	0.0177	0.0020	48.31	<0.0001 **	0.1588	0.0176	106.93	<0.0001 *
A	0.0087	0.0087	212.23	<0.0001 **	0.0974	0.0974	590.31	<0.0001 *
B	0.0009	0.0009	22.01	0.0009 **	0.0143	0.0143	86.41	<0.0001 *
C	0.0068	0.0068	166.22	<0.0001 **	0.0277	0.0277	168.11	<0.0001 *
AB	5.029×10^{-8}	5.029×10^{-8}	0.0012	0.9727 ns	0.0001	0.0001	0.4495	0.5178 ns
AC	4.155×10^{-6}	4.155×10^{-6}	0.1019	0.7562 ns	5.665×10^{-6}	5.665×10^{-6}	0.0343	0.8567 ns
BC	0.0002	0.0002	3.72	0.0828 ns	0.0012	0.0012	7.34	0.0219 *
A^2	0.0007	0.0007	18.33	0.0016 *	0.0083	0.0083	50.53	<0.0001 **
B^2	0.0000	0.0000	0.9071	0.3633 ns	0.0006	0.0006	3.61	0.0865 ns
C^2	0.0000	0.0000	0.2896	0.6023 ns	0.0011	0.0011	6.49	0.0290 *
Residual	0.0004	0.0000			0.0016	0.0002		
Lack of Fit	0.0004	0.0001	3.70	0.0885 ns	0.0016	0.0003	1.65	0.2980 ns
Pure Error	0.0000	0.0000			0.0000	0.0000		
Cor Total	0.0181				0.1604			
C.V. %	7.64				3.37			

Note: *, **, and ns denote 5% and 1% levels of significance and not significant, respectively.

Moreover, the ANOVA test distinctly indicated that EU was remarkably affected by the linear terms of drying air temperature (A), drying air velocity (B), and infrared power (C) ($p < 0.01$), whereas the interaction terms of AB, AC, and BC did not have significant effects on EU ($p > 0.05$). Regarding the square terms of the EU response, it was concluded that, except for the quadratic-degree effect of drying air temperature (A^2) ($p < 0.05$), the rest of the quadratic-degree terms (B^2 and C^2) had no significant effects on energy utilisation (EU) (Table 5). In the present study, according to the results for EUR, the variable A (drying air temperature) was found to be very significant with a p-value < 0.0001, followed by B (drying air velocity) and C (infrared power). In addition, the model's interaction terms (AB and AC), except for AC, were not significant in predicting EUR during the drying process ($p > 0.05$). Among the quadratic terms of the model to predict EUR, the term A^2 had a highly significant effect with $p < 0.0001$, and the term C^2 with p = 0.02 also had a significant influence on EUR. Additionally, it was not affected by the quadratic term of drying air velocity (B^2) ($p > 0.05$), as shown in Table 5.

Moreover, an analysis of the tests was performed using the Design–Expert software to obtain the most suitable mathematical model for the prediction of the responses, such as EU and EUR. Cubic polynomial, linear, dual-factor (2F1), and quadratic model interactions were examined. To evaluate the adequacy of the model, the values of the statistical parameters of R^2, Pre-R^2, and Adj-R^2, and the adequate precision were all identified. Among the available models, the quadratic model was selected as the best model to predict the parameters of EU and EUR using RSM modelling. Table 6 shows that the three important coefficients of regression ($R^2 > 0.97$, predicted $R^2 > 0.78$, and adjusted $R^2 > 0.95$, with (adjusted R^2-predicted R^2) <0.2, for the prediction of EU, and $R^2 > 0.98$, pred. $R^2 > 0.95$, adj. $R^2 > 0.98$, with (adjusted R^2-predicted R^2) <0.2, for the prediction of EUR) prove that these models are able to explain most of the observed variation. In addition, the high value of $R^2 = 0.9775$ implied that only 2.25% of the total variation could not be explained by the quadratic model for EU, while this value was 1.03% for EUR. EU and EUR had an adequate precision higher than 4, representing sufficient discrimination of the models. Adequate precision evaluates the signal to the ratio of noise that is reasonably higher than 4 [47]. The values of adequate precision for EU and EUR were 28.75 and 41.64, respectively, while the values of PRESS for the selective model were found to be 0.0038 and 0.0078, respectively (Table 6). The ratios of 28.75 and 41.64 for EU and EUR represented an adequate signal, so these models could be utilised to navigate the space of design [47].

Table 6. Summarised statistical data of the predictive models for energy utilisation and energy utilisation ratio.

Source	Std. Dev.	R^2	Adj. R^2	Pred. R^2	PRESS	Adeq Precision	
EU						28.75	
Linear	0.0106	0.9003	0.8816	0.8364	0.0030		
2FI	0.0113	0.9089	0.8669	0.5754	0.0077		
Quadratic	0.0064	0.9775	0.9573	0.7878	0.0038		Suggested
Cubic	0.0039	0.9950	0.9843	−5.1028	0.1107		Aliased
EUR						41.64	
Linear	0.0363	0.8689	0.8443	0.7907	0.0336		
2FI	0.0390	0.8769	0.8201	0.4186	0.0933		
Quadratic	0.0128	0.9897	0.9805	0.9515	0.0078		Suggested
Cubic	0.0161	0.9903	0.9692	−10.9502	1.92		Aliased

Through the utilisation of multiple regression assessment on the drying experimental data, the following quadratic polynomial equations were found to indicate energy utilisation and energy utilisation ratio:

$$EU = 0.0911 + 0.0294A + 0.0095B + 0.0260C − 0.0165A^2 \tag{27}$$

$$EUR = 0.4111 + 0.0987A + 0.0378B + 0.0527C + 0.0123BC − 0.0535A^2 − 0.0197C^2 \tag{28}$$

where A, B, and C are the coded values of drying air temperature, drying air velocity, and infrared power in the equations. The positive and negative coefficients of the model terms depict synergistic and antagonistic effects on the energy utilisation and energy utilisation ratio of terebinth drying, respectively. In these cases, A, B, C, and A^2 are the significant terms of the quadratic model for predicting EU, whereas BC and C^2 are the significant terms of this model to predict EUR in addition to the terms A, B, C, and A^2. The quadratic term of drying air temperature has an affirmative effect on EU and EUR, with the highest positive values of coefficient equal to 0.0294 and 0.098, respectively, whereas drying air velocity has the lowest effect on EU and EUR among the independent variables.

As illustrated in Figure 3a,c, the plots of normal probability for residual distribution of the given responses (EU and EUR) are used to benchmark the RMS model accuracy. The external residuals commonly decline in a straight line, showing that the residual distribution is in the range of normal, and the least-squares fitting adequacy is confirmed (Figure 3a,c). In addition, it shows that the relevant models are suitable for predicting the responses. Moreover, Figure 3b,d demonstrate that the values of Lambda, which signify the power given to the values corresponding to the response variables, are −0.54 and 0.60, respectively, which then have a Lambda value of 1.0 after power transformation. Overall, the plots in Figure 3 identify which of the developed regression models of energy utilisation and energy utilisation ratio with good performance in the goodness of fit test align with the predictions of the ANOVA test during a fluidised bed-infrared drying process of terebinth fruit. Similar findings have been observed by Gorji and Ranjbar [48] while optimising a nanofluid-based direct absorption solar collector.

3.2.2. Impact of Drying Conditions on EU and EUR

To assess the interactions between drying air temperature, drying air velocity, and infrared power on the responses of EU and EUR, three-dimensional plots of the response surface were constructed for each of the relevant models on the performance of the three independent parameters (Figure 4a–d). This distinct surface supplies the system's EU and EUR at any point of the suggested range for the experiment's factors.
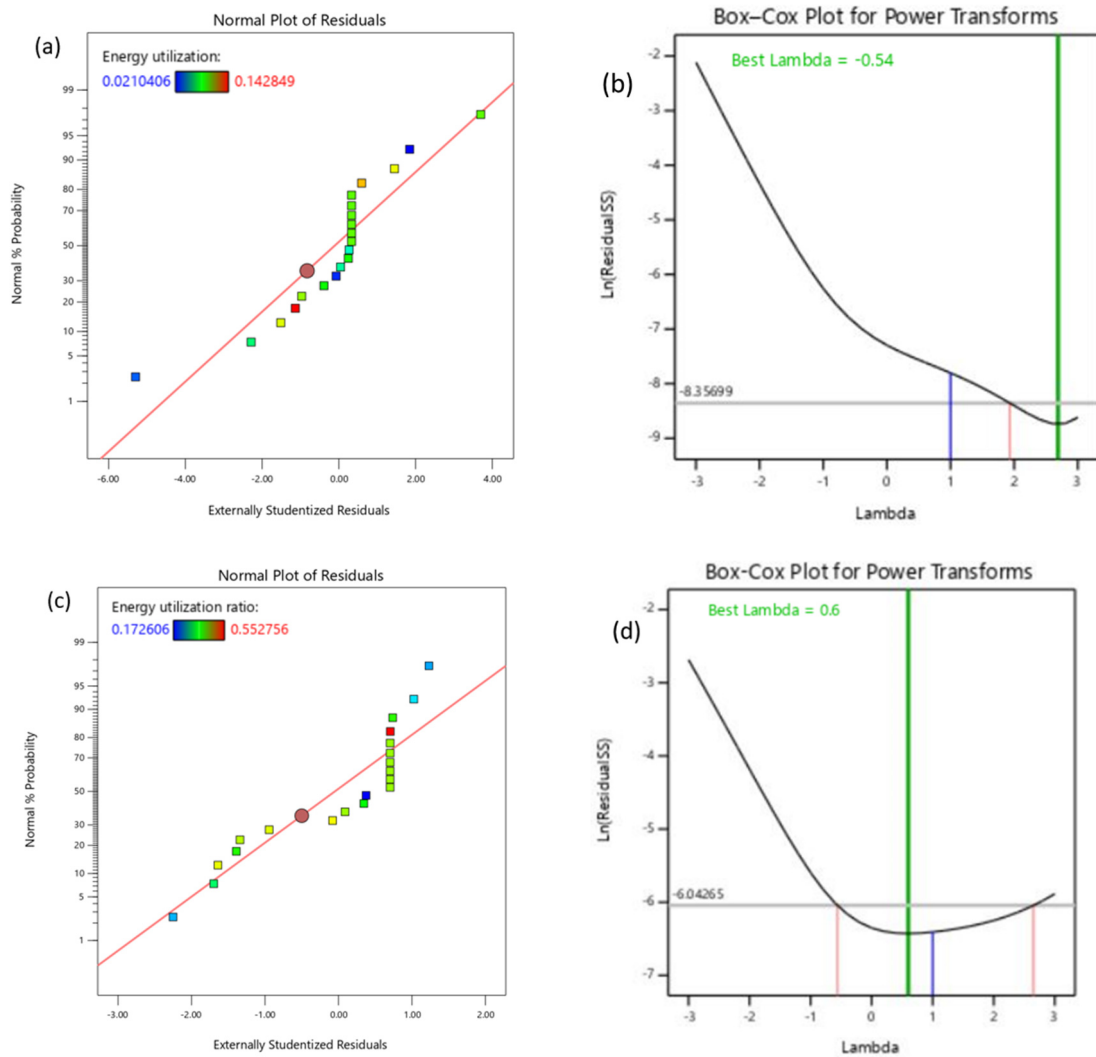
Figure 3. Diagnostic plots for the optimisation process of the FBI dryer during terebinth drying: (**a**) normal probability plot of residuals for EU, (**b**) Box–Cox plot after power transformation of EU, (**c**) normal probability plot of residuals for EUR, and (**d**) Box–Cox plot after power transformation of EUR.
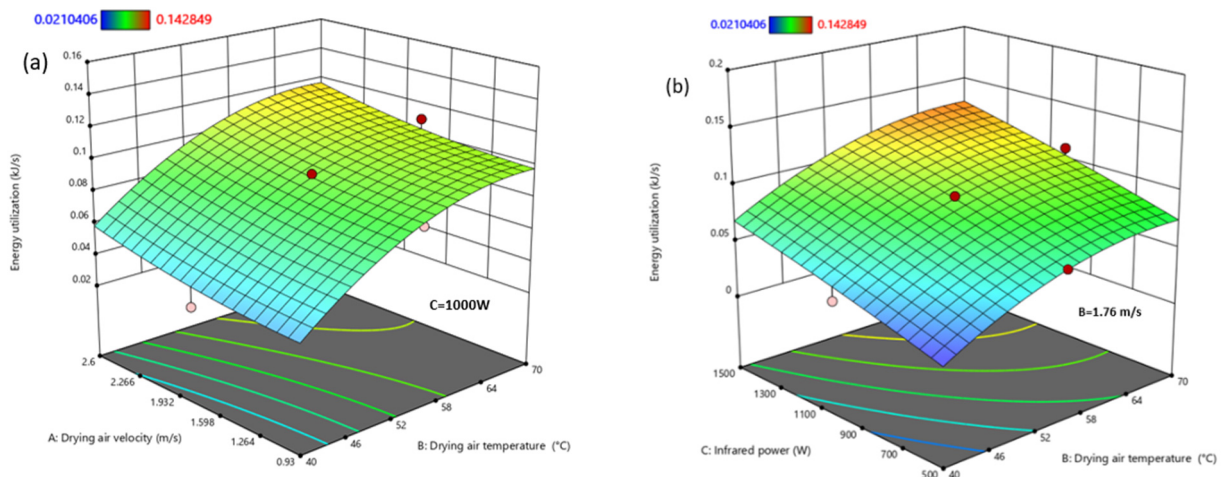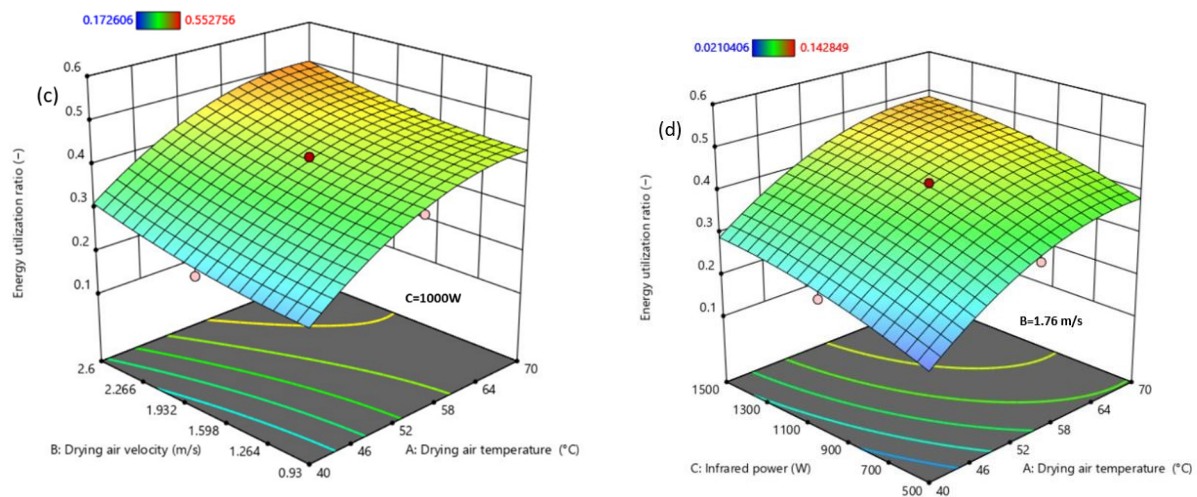

Figure 4. *Cont*.

Figure 4. Response surface plot interaction between (**a**) air velocity and drying air temperature on energy utilisation, (**b**) infrared power and air temperature on energy utilisation, (**c**) air velocity and drying air temperature on energy utilisation ratio, and (**d**) infrared power and drying air temperature on energy utilisation ratio.

Figure 4a implies that EU is a function of drying air temperature, drying air velocity and infrared power. In Figure 4a,b, it can be shown that these independent variables simultaneously have a significant effect on EU. EU increases with rising drying air temperature, drying air velocity, and infrared power, and decreases with drying time. Enhancing drying air temperature increases the rate of heat transfer from wall to gas and from gas to solid, which leads to a rise in the rate of moisture evaporation that results in more energy utilisation in a dryer [49]. In Figure 3a,b, the red colour shows that the maximum value of EU (0.142 kJ/s) occurs at a drying air temperature of 70 °C, drying air velocity of 2.60 m/s, and infrared power of 1500 W, whereas the lowest value (0.021 kJ/s) occurs at 40 °C drying air temperature, 0.93 m/s drying air velocity, and 500 W infrared power. The EU of the terebinth samples in the FBI dryer of this study is lower than that of a microwave dryer in the study conducted by Motevali and Minaei [50] to dry sour pomegranate arils. The same findings in terms of the influences of drying air temperature and air velocity on EU have been reported by Beigi [51] for drying kiwifruit slices. However, it can be observed that the minimum EU occurs near high air temperatures at a constant air velocity value of 1.76 m/s for all levels of infrared power. Furthermore, the drying air temperature has a greater effect on EU than other independent variables. As presented in Figure 4c,d, it can be seen that EUR also increases with the three independent variables, including drying air temperature, drying air velocity, and infrared power. The influences of drying air temperature and infrared power are more significant than the influence of air velocity on EUR. The minimum value of EUR is 0.172 kJ/s for terebinth drying at a drying air temperature of 40 °C, a drying air velocity of 0.93 m/s, and infrared power of 500 W. The maximum value of 0.552 kJ/s is obtained at 70 °C with a drying air velocity of 2.60 m/s and infrared power of 1500 W (Figure 4c,d). Moreover, the results obtained in this study are similar to those of Golpour et al., [22], Corzo et al., [52], and Aghbashlo et al., [34], who found that EU rises with increasing drying air temperature and air velocity.

3.3. Evaluation of EX_{eff} and Ex_{loss}

3.3.1. The Model Analysis and Assessment for EX_{eff} and Ex_{loss}

Table 7 shows the results of the variance analysis regarding the statistical significance of linear, quadratic, and interactive influences of the independent factors (drying air temperature, drying air velocity, and infrared power) on EX_{eff} and Ex_{loss}. The results show that the values of "Prob. > F" confirm the predicted EX_{eff} and Ex_{loss} relationships. The F-value for the models of the responses (exergetic efficiency and exergy loss rate) were

152.74 and 66.17, respectively, while the values of the lack of fit test were not significant and the coefficient of determination (R^2) was acceptable for both of the responses, showing that the extracted models were suitable (Table 7). The *p*-values of the models for predicting EX_{eff} and Ex_{loss} were less than 0.0001, showing that the terms of the models were highly significant (Table 7). With such high values of F in the prediction of EX_{eff} and EX_{loss}, there was only a possibility of 0.01% that this could have been because of noise [53]. Overall, the greater F-value demonstrates the higher reliability of the models, whereas the significance of the models is identified with lower *p*-values [54,55]. In the present study, the obtained results of the ANOVA test of exergetic efficiency (EX_{eff}) and exergy loss rate (Ex_{loss}), as illustrated in Table 7, affirm that the independent parameters of drying air velocity, air temperature, and infrared power are statistically significant with $p < 0.01$. According to the results of Table 7, it can be shown that only A^2 and AC are significant in addition to the linear terms with *p*-value < 0.05. There are no significant effects for the rest of the terms of the model in the prediction of exergetic efficiency ($p > 0.05$) (Table 7). This shows that drying air temperature (A) has a stronger influence on EX_{eff} optimisation. Moreover, only the linear terms are significant in predicting the exergy loss rate, and other interactive and quadratic terms (AB, AC, BC, A^2, B^2, and C^2) have no significant effects on the exergy loss rate.

Table 7. ANOVA results of the quadratic model factors of the RSM on the responses of exergetic efficiency and exergy loss rate.

	EX_{eff}				EX_{loss}			
Source	**SS**	**MS**	**F-Value**	**p-Value**	**SS**	**MS**	**F-Value**	**p-Value**
Model	1313.73	145.97	152.74	<0.0001 **	0.0083	0.0028	66.17	<0.0001 **
A	812.94	812.94	850.63	<0.0001 **	0.0029	0.0029	69.27	<0.0001 **
B	199.78	199.78	209.05	<0.0001 **	0.0014	0.0014	33.26	<0.0001 **
C	221.79	221.79	232.08	<0.0001 **	0.0040	0.0040	95.99	<0.0001 **
AB	4.46	4.46	4.66	0.0562 ns				
AC	25.18	25.18	26.35	0.0004 **				
BC	1.43	1.43	1.50	0.2487 ns				
A^2	25.37	25.37	26.54	0.0004 **				
B^2	0.1576	0.1576	0.1649	0.6933 ns				
C^2	0.0529	0.0529	0.0553	0.8188 ns				
Residual	9.56	0.9557			0.0007	0.0000		
Lack of Fit	9.56	1.91	1.59	0.3110 ns	0.0007	0.0001	3.54	0.871 ns
Pure Error	0.0000	0.0000			0.0000	0.0000		
Cor Total	1323.29				0.0089			
C.V. %	1.40				13.13			

Note: ** and ns denote 1% level of significance and not significant, respectively.

The statistical values of the best-fitting models according to the ANOVA test are presented in Table 8 in the prediction of exergetic efficiency and exergy loss rate. As shown in Table 8, the quadratic model for exergetic efficiency, with $R^2 = 0.9928$, an adjusted coefficient of $R^2 = 0.9863$, and a predicted coefficient of $R^2 = 0.9584$, has better performance than the other models, due to this model having a value difference between the adjusted and predicted coefficients of less than 0.20 [56]. The linear model is the best to predict the exergy loss rate with the values of 0.9254, 0.9114, and 0.8581 for the parameters of R^2, Adj. R^2, and Pred. R^2, respectively (Table 8). According to the R^2 obtained, only 0.82% and 8.46% of the total variation cannot be explained by the RSM model for EX_{eff} and EX_{loss}, respectively. The fit of the models was tested using ANOVA, and the obtained results demonstrated that the corresponding equation correctly reproduced the real relationship between a set of independent parameters and the responses (Table 8). Although the predicted sum of squares (PRESS) of 55.09 and 0.0013 were optimal for the selected model, the relatively low value of CV indicated that the test data had good reliability (Table 8). Moreover, the values of adeq. precision for Ex_{eff} and Ex_{loss} were 52.64 and 33.78, respectively. Adeq. precision

values show the proportion of experimental input factors and noise, and a proportion > 4 is satisfactorily acceptable [57].

Table 8. Summarised statistical data of the predictive models for exergetic efficiency and exergy loss rate.

Source	Std. Dev.	R^2	Adj. R^2	Pred. R^2	PRESS	Adeq Precision	
Ex$_{eff}$						52.64	
Linear	2.36	0.9329	0.9203	0.8777	161.90		
2FI	2.11	0.9564	0.9363	0.8022	261.80		
Quadratic	0.9776	0.9928	0.9863	0.9584	55.09		Suggested
Cubic	0.9575	0.9958	0.9868	−4.1073	6758.38		Aliased
Ex$_{loss}$						33.78	
Linear	0.0064	0.9254	0.9114	0.8581	0.0013		Suggested
2FI	0.0056	0.9543	0.9332	0.7816	0.0019		
Quadratic	0.0046	0.9763	0.9549	0.7637	0.0021		
Cubic	0.0018	0.9979	0.9934	−1.5465	0.0227		Aliased

A predictive regression model was developed using RSM to correlate the responses of exergetic efficiency and exergy loss rate with the input factors, and their regression coefficients in coded terms are presented in Equations (29) and (30):

$$EX_{eff} = 68.23 - 9.02A + 4.47B - 4.71C - 1.77AC + 3.04A^2 \tag{29}$$

$$EX_L = 0.0491 + 0.0170A + 0.0118B + 0.0200C \tag{30}$$

Equation (29) states the second-order quadratic model of exergy efficiency. In this case, T, V, and P are highly significant model terms that are statistically significant at $p < 0.05$. Therefore, from Equation (29), infrared power with the lowest negative coefficient of −4.71 among the independent terms is the most ineffective factor for increasing exergy efficiency. Based on Equation (30), the most effective factor for decreasing the exergy loss rate is infrared power, which has the highest positive coefficient of 0.0200. In addition, the square and interactive effects of the independent factors are not significant in the prediction of exergy loss rate according to this model ($p \geq 0.05$).

The plots in Figure 5a,c illustrate the adequacy of the models in the prediction of exergetic efficiency and exergy loss rate, respectively. The results show that the vicinity of the observed data to the line of fitting illustrates a considerable relationship between the estimated and observed data (Figure 5a,c). Thus, the extracted relation of the models to predict the responses has the ability to predict the observed data accurately with a satisfactory normal distribution. Indeed, it can be seen in Figure 5a,c that the residuals fall in a straight line, which depicts that the obtained errors are commonly distributed. The Box–Cox plots validate the prediction accuracy of the corresponding models through the power transformation of exergetic efficiency and exergy loss rate to the value of Lambda = 1.00, with residual dispersion randomly between −3 to 3 in the related domain. The values of Lambda, which specify the power given to the variables of response, are 3.00 and 0.88 for EX$_{eff}$ and Ex$_{loss}$ after power transformation with a value of Lambda = 1, as shown in Figure 5b,d. Thus, the developed relations for EX$_{eff}$ and Ex$_{loss}$ have the ability to faithfully predict the observed data.

3.3.2. Impact of Drying Conditions on EX$_{eff}$ and Ex$_{loss}$

The 3D plots of the responses, namely exergy efficiency and exergy loss rate under the interactions of drying air temperature, drying air velocity, and infrared power, during the drying process of the terebinth samples are shown in Figure 6a–d. The exergy efficiency for the hybrid convective drying of terebinth for the different conditions was obtained in the range of 50.57–87.57% (Figure 6a,b). The obtained results showed that exergy efficiency declined with rising drying air temperature from 40 °C to 70 °C and infrared power from 500 W to 1500 W, while this response increased with rising air velocity from 0.93 to

2.60 m/s. Exergetic efficiency can be computed using Equation (17) on the basis of exergy inflow, outflow, and losses. The drying air temperature difference between the FBI dryer and the environment was great, causing low exergy efficiency [58]. On the other hand, exergy efficiency declined with rising drying air temperature because of the great exergy losses. Thus, the highest value of exergy efficiency obtained was 87.57% at 40 °C drying air temperature, 2.60 m/s air velocity, and 500 W infrared power, and the lowest value of this response was 50.57% at drying air temperature of 70 °C, drying air velocity of 0.93 m/s, and infrared power of 1500 W (Figure 6a,b). However, the obtained value for exergy efficiency in the present study was less than the exergy efficiency of dried carrot samples in a semi-industrial continuous band dryer reported by Aghbashlo et al. [34]. Therefore, these values for exergy efficiency clearly specify the outflow of the FBI dryer system as the main site of thermodynamic inefficiency, illustrating that a great proportion of thermal exergy provided is lost in the outlet air and dryer frame in the case of the dryer in this study. The results of this study show that great exergetic efficiency is due to low drying air velocity. Hence, the exergy inflow to the FBI dryer comes out again as an outflow of exergy along with air velocity, which is named low exergy consumption [58].
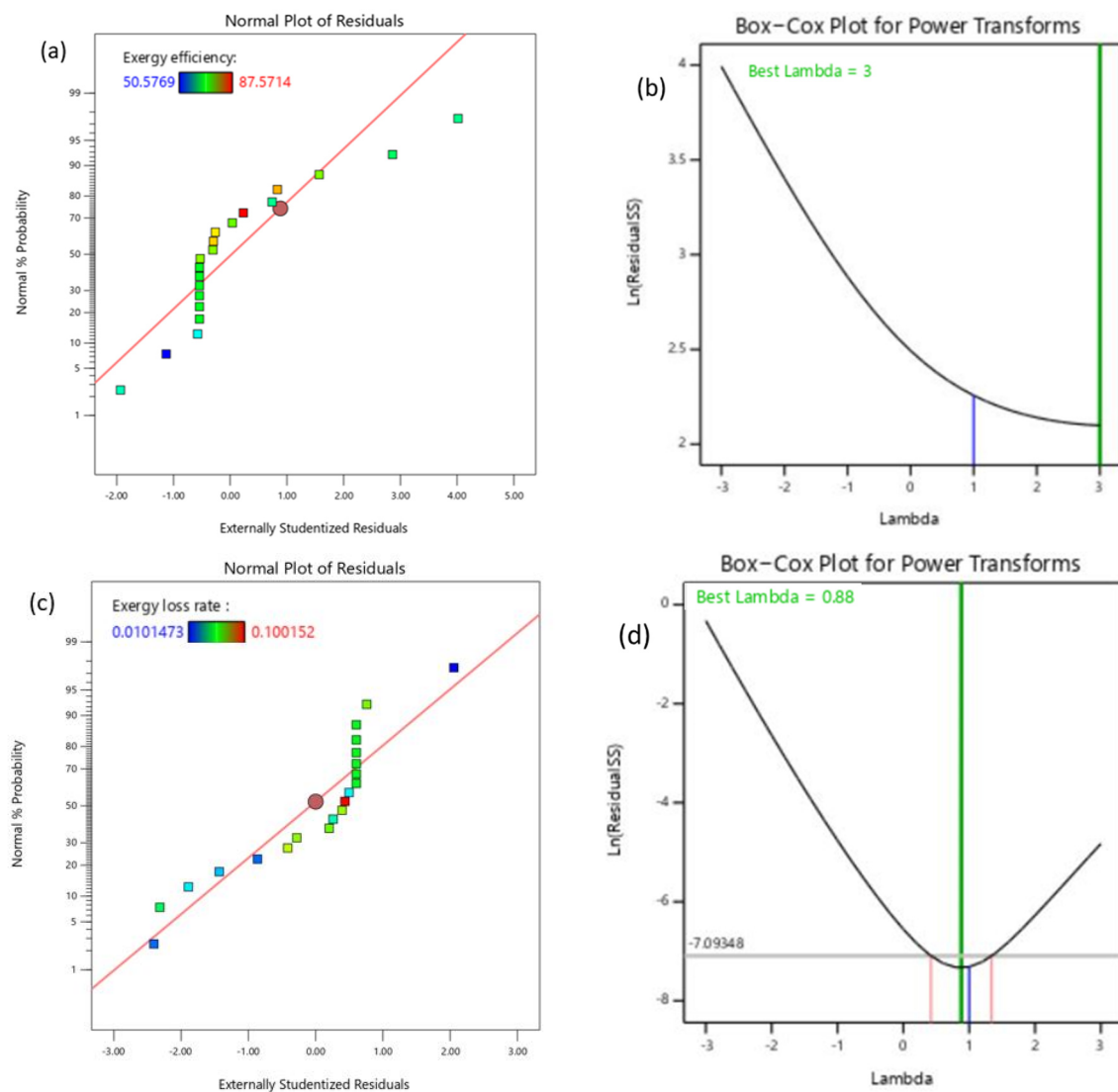

Figure 5. Diagnostic plots for the optimisation process of the FBI dryer during terebinth drying: (**a**) normal probability plot of residuals for EX_{eff}, (**b**) Box–Cox plot after power transformation of EX_{eff}; (**c**) normal probability plot of residuals for Ex_{loss}, and (**d**) Box–Cox plot after power transformation of EX_{loss}.
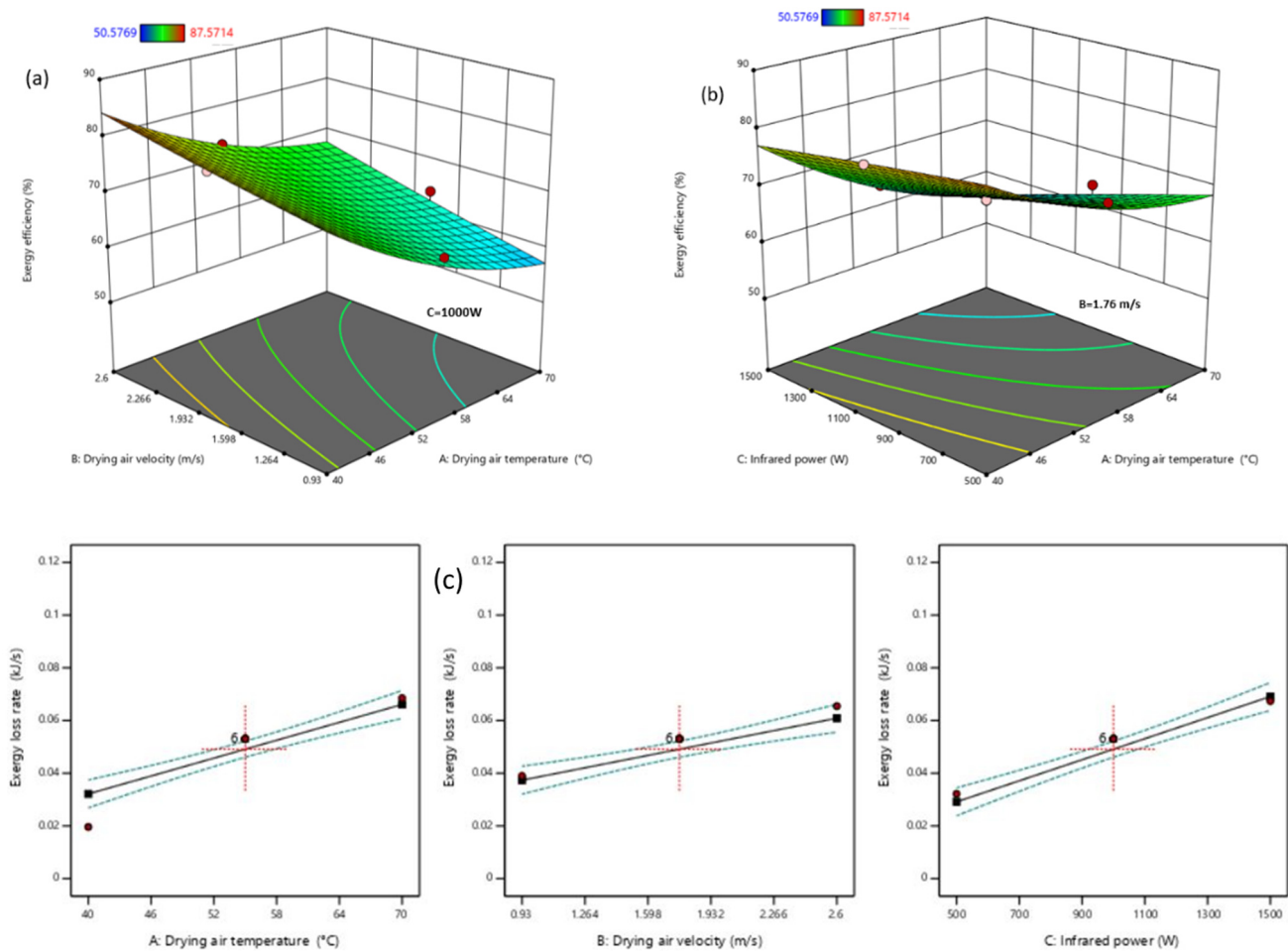
Figure 6. Response surface plot interaction between (**a**) air velocity and air temperature on exergetic efficiency, and (**b**) infrared power and air temperature on exergetic efficiency. (**c**) Linear plot of air temperature, air velocity, and infrared power on exergy loss rate.

Moreover, the graphical results in Figure 6c show that exergy loss rate increases with an increase in all three independent factors, including drying air temperature, drying air velocity, and infrared power, showing that these factors have an effective influence on the related responses. According to the extracted results, the maximum value of exergy loss rate (0.100 kJ/s) occurred at a drying air temperature of 70 °C, a drying air velocity of 2.60 m/s, and infrared power of 1500 W during the FBI drying process of terebinth (Figure 6c). Exergy loss increases with higher air velocity because of an increase in gas–solid heat transfer rate, leading to more evaporation of moisture. This enhances the available energy at the outlet of the dryer, so raising the exergy outlet of the dryer. Moreover, in the present study, exergy loss rate rose with an increase in drying air temperature during the drying process of terebinth. The same observations were found in the study by Corzo et al. [52] during the drying of corobo slices in a micro-oven. The exergy loss rate was found to be greater at the beginning of the drying process due to the evaporation of more moisture from the terebinth samples and then declined with respect to drying time [49]. Hence, the exergy loss rate from the FBI dryer frame could be decreased by prohibiting heat transfer rate across the system's boundary. Sealing the FBI dryer body, insulating the FBI dryer frame, designing and selecting suitable components, and supplying the optimal drying conditions could assist in diminishing exergy loss rate and raise the efficiency of thermodynamics for this kind of industrial dryer.

3.4. Evaluation of $I\dot{P}$ and SI

3.4.1. The Model Analysis and Assessment for $I\dot{P}$ and SI

Table 9 shows the variance analysis of the linear and interaction effects of the independent variables on $I\dot{P}$ and SI. From the results in this Table, it is clear that the lower the *p*-value, the more important the model terms are. The F-value for the $I\dot{P}$ and SI models were 297.95 and 64.67, respectively, and the *p*-value for all the selected models was <0.0001, suggesting that the models were significant (Table 9). As shown in Table 9 for $I\dot{P}$ and SI, the *p*-values of the fitted models are significant, indicating their importance in relation to the input parameters of drying air temperature, drying air velocity, and infrared power. Furthermore, in Table 9, the results of $I\dot{P}$ for terebinth drying indicate the significance of the linear terms A, B, and C, and the interactive terms AB, AC, and BC (*p*-value < 0.01). In contrast, other terms, including all the quadratic terms A^2, B^2, and C^2, are not significant, so reducing the model could have a positive effect on improving the model [59] (*p* > 0.05) (Table 9). In addition, due to the lack of fit and its non-significance, the coefficient of variation for this statistical analysis of $I\dot{P}$ and SI and the input parameters were 3.83% and 6.61%, respectively, showing that the obtained models have good performance in predicting $I\dot{P}$ and SI. In addition, from Table 9 for the response of SI, it can be observed that the linear coefficients of these input factors and the interaction terms, except for AC, have a highly significant effect on the RSM model of SI with *p*-value < 0.01, whereas the second-order coefficients (B^2 and C^2) have *p*-values greater than 0.05, showing that they are not significant (*p* > 0.05) (Table 9). Moreover, considering the *p*-values for optimisation, it can be shown that the interaction effects of AB and BC have a higher impact on SI, whereas the *p*-value in the term coefficient of AC is >0.05 (Table 9). Generally, based on the results obtained and the model, drying air temperature (A), drying air velocity (B) and infrared power (C) have a very significant effect on $I\dot{P}$ (*p*-value < 0.0001), showing the functions of these responses are validated from the view point of statistical approach [48].

Table 9. ANOVA results of the 2FI model factors of the RSM on the responses of exergetic improvement potential rate and sustainability index.

	$I\dot{P}$				SI			
Source	**SS**	**MS**	**F-Value**	**_p_-Value**	**SS**	**MS**	**F-Value**	**_p_-Value**
Model	31.60	5.27	297.95	<0.0001 **	33.52	3.72	64.67	<0.0001 **
A	13.29	13.29	751.91	<0.0001 **	17.18	17.18	298.39	<0.0001 **
B	6.87	6.87	388.62	<0.0001 **	5.24	5.24	91.06	<0.0001 **
C	9.81	9.81	555.25	<0.0001 **	4.51	4.51	78.36	<0.0001 **
AB	0.7059	0.7059	39.94	<0.0001 **	1.13	1.13	19.58	0.0013 **
AC	0.7306	0.7306	41.34	<0.0001 **	0.3534	0.3534	6.14	0.0327 *
BC	0.1886	0.1886	10.67	0.0061 **	0.8064	0.8064	14.00	0.0038 **
A^2	-	-			1.51	1.51		0.0005 **
B^2	-	-			0.0554	0.0554		0.3499 ns
C^2	-	-			0.0521	0.0521		0.3640 ns
Residual	0.2298	0.0177			0.5759	0.0576		
Lack of Fit	0.2298	0.0287	2.56	0.1582 ns	0.5759	0.1152	2.84	0.1380 ns
Pure Error	0.0000	0.0000			0.0000	0.0000		
Cor Total	31.82				34.10			
C.V. %	3.83				6.61			

Note: *, ** and ns denote 5 and 1% levels of significance and not significant, respectively.

Table 10 demonstrates that the 2FI and quadratic models result in a better prediction of exergetic improvement potential rate and sustainability index in relation to other models. The selected model (2FI) for exergetic improvement potential rate evaluates the determination (R^2) coefficient, adjusted R^2, predicted R^2, and adequate precision. The R^2 value of 0.9928 shows that the model could affirm 99.28 % of the variation in the experi-

mental data but does not affirm 0.72% of the overall differences (Table 10). For a suitable model, the R^2 values should not be lower than 0.75 [60]. The values of adj-R^2 = 0.9894, pred-R^2 = 0.9758, and Adeq Precision = 75.57 show the acceptable performance of the 2FI model in the prediction of exergetic improvement potential rate, as illustrated in Table 10. These results are in agreement with the results reported by Benhamza et al. [31] for a $I\dot{P}$ model in a solar air heater for food drying. Furthermore, the quadratic model selected for sustainability index has a determination coefficient (R^2) of 0.9831, adj-R^2 of 0.9679, and pred-R^2 of 0.8001, which are in acceptable agreement as their difference is lower than 0.20 [61,62]. Additionally, a high value of determination coefficient (R^2 = 0.9831) in the range of the desired model shows that 1.69% of the total variation cannot be explained by the RSM model. Furthermore, the adequate precision value of 31.90 is more than 4, indicating that the relevant SI model has adequate signal to noise and could be utilised to navigate the space of design [61]. Moreover, the obtained values of pred-sum of square (PRESS) of 0.7689 and 6.82 are favourable for predicting $I\dot{P}$ and SI, respectively.

Table 10. Summarised statistical data of the predictive models for exergetic improvement potential rate and sustainability index.

Source	Std. Dev.	R^2	Adj. R^2	Pred. R^2	PRESS	Adeq Precision	
$I\dot{P}$						75.57	
Linear	0.3405	0.9417	0.9308	0.8680	4.20		
2FI	0.1329	0.9928	0.9894	0.9758	0.7689		Suggested
Quadratic	0.1283	0.9948	0.9902	0.9588	1.31		
Cubic	0.0204	0.9999	0.9998	0.9039	3.06		Aliased
SI						31.90	
Linear	0.6687	0.7902	0.7508	0.5929	13.88		
2FI	0.6118	0.8573	0.7914	0.0384	32.78		
Quadratic	0.2400	0.9831	0.9679	0.8001	6.82		Suggested
Cubic	0.0449	0.9996	0.9989	0.5650	14.83		Aliased

Equations (31) and (32), which encode the independent parameters of air temperature (A), air velocity (B), and infrared power (C), are the final equations for the regression model representing the responses to exergetic improvement potential rate and sustainability index, respectively. These obtained models were mainly used to determine the optimal drying conditions in the evaluation of the optimisation modelling, which included the linear, quadrative and interactive effects of the independent variables on these responses. The positive signs in the obtained models showed synergetic influences, whereas the negative signs demonstrated antagonistic influences of the variables. In this way, the 2FI and quadratic models were obtained with good fit and could be used to describe the changes in $I\dot{P}$ and SI, in which air temperature with the highest positive coefficient (1.15) was the most important factor in predicting this response, and air velocity had less significance among the independent factors with a coefficient value of 0.8287 in the $I\dot{P}$ model. Infrared power, with the greatest negative coefficient of −0.671, was the most effective factor in increasing the sustainability index.

$$I\dot{P} = 3.47 + 1.15A + 0.8287B + 0.9906C + 0.2970AB - 0.3022AC + 0.1535BC \tag{31}$$

$$SI = 3.12 - 1.31A + 0.7242B - 0.6718C - 0.3755AB + 0.2102AC - 0.3175BC + 0.7398A^2 \tag{32}$$

The pattern of the distributing data was assessed for $I\dot{P}$ and SI by examining the plots of two parameters, namely the normal % probability and related studentised residuals (Figure 7a,c). The plots demonstrate that the obtained experimental values are closely equal to the predicted values in a straight line and validate the suitability of the developed models to predict $I\dot{P}$ and SI. The accuracy of prediction for the obtained models of $I\dot{P}$ and SI was examined using the Box–Cox plots (Figure 7b,d) after the transformation of power for Lambda value equal to 1 for these parameters. It was obvious that the 2FI and quadratic

models had the ability to predict nearly perfectly the experimental data and could clarify 99.28% and 98. 31% of the changes in the $I\dot{P}$ and SI of the terebinth samples in the hybrid infrared dryer.
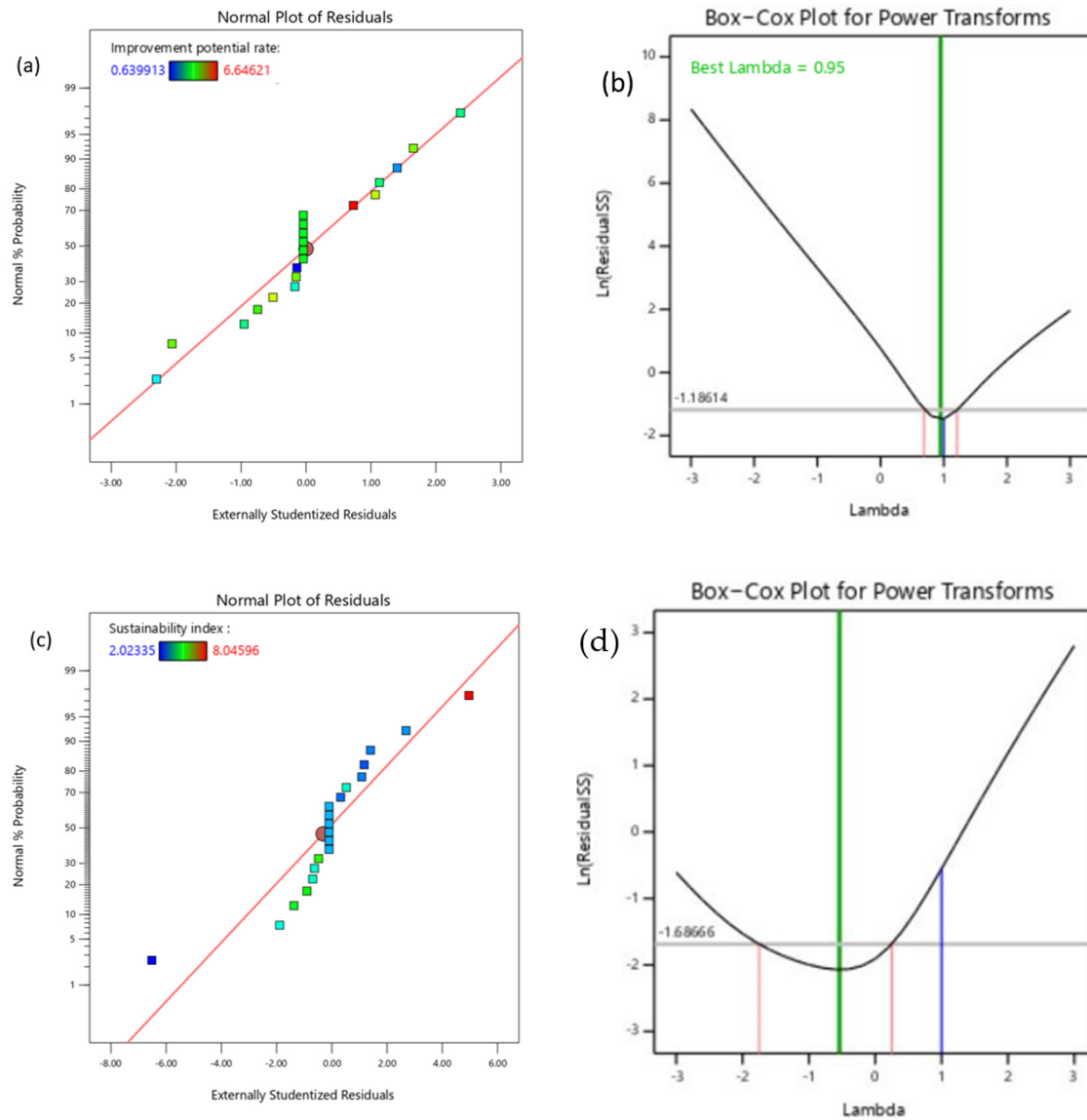

Figure 7. Diagnostic plots for the optimisation process of the FBI dryer during terebinth drying: (**a**) normal probability plot of residuals for $I\dot{P}$, (**b**) Box–Cox plot after power transformation of $I\dot{P}$, (**c**) normal probability plot of residuals for SI, and (**d**) Box–Cox plot after power transformation of SI.

3.4.2. Impact of Drying Conditions on $I\dot{P}$ and SI

Three-dimensional surface plots of T, V, and P were examined to visualise the combined influence of the important factors of the drying process of terabinth on $I\dot{P}$ and SI, as shown in Figure 8a–d. According to the obtained results, amongst the input factors, drying air temperature was the most significant parameter of the drying process that influenced the response of $I\dot{P}$. Accordingly, at a high temperature (70 °C), the greatest $I\dot{P}$ attained was 6.646 kJ/s when drying air velocity and infrared power were 2.60 m/s and 1500 W, respectively, whereas the lowest value of $I\dot{P}$ was predicted to be 0.639 kJ/s at 40 °C drying air temperature, 0.93 m/s drying air velocity, and 500 W infrared power for the FBI dryer. However, the values of the improvement potential rate varied from 0.639 kJ/s to 6.646 kJ/s under the operating conditions, which were comparable to the results reported

by Alhanif et al. [58] for drying papaya seeds (0.001 to 4.45 kJ/kg). Moreover, the positive coefficients of T, V, and P in Equation (31) suggest that $I\dot{P}$ increases with an increase in the three independent factors (drying air temperature, air velocity, and infrared power) (Figure 8a,b). Aghbashlo et al. [63] and Okunola et al. [9] reported similar findings on the drying of encapsulated fish oil and okra, respectively. One approach to enhance the value of exergy improvement potential rate is to diminish the irreversible process in the form of exergy consumption, which can be practically performed by applying lower drying air temperatures. In addition, pinch technology to a heat exchanger can be another application to improve this exergy parameter. Anyway, existing small temperature difference (ΔT) between hot and cold flows can decline the parameter of irreversibility, which enhances the amount of exergy that can be used [58].
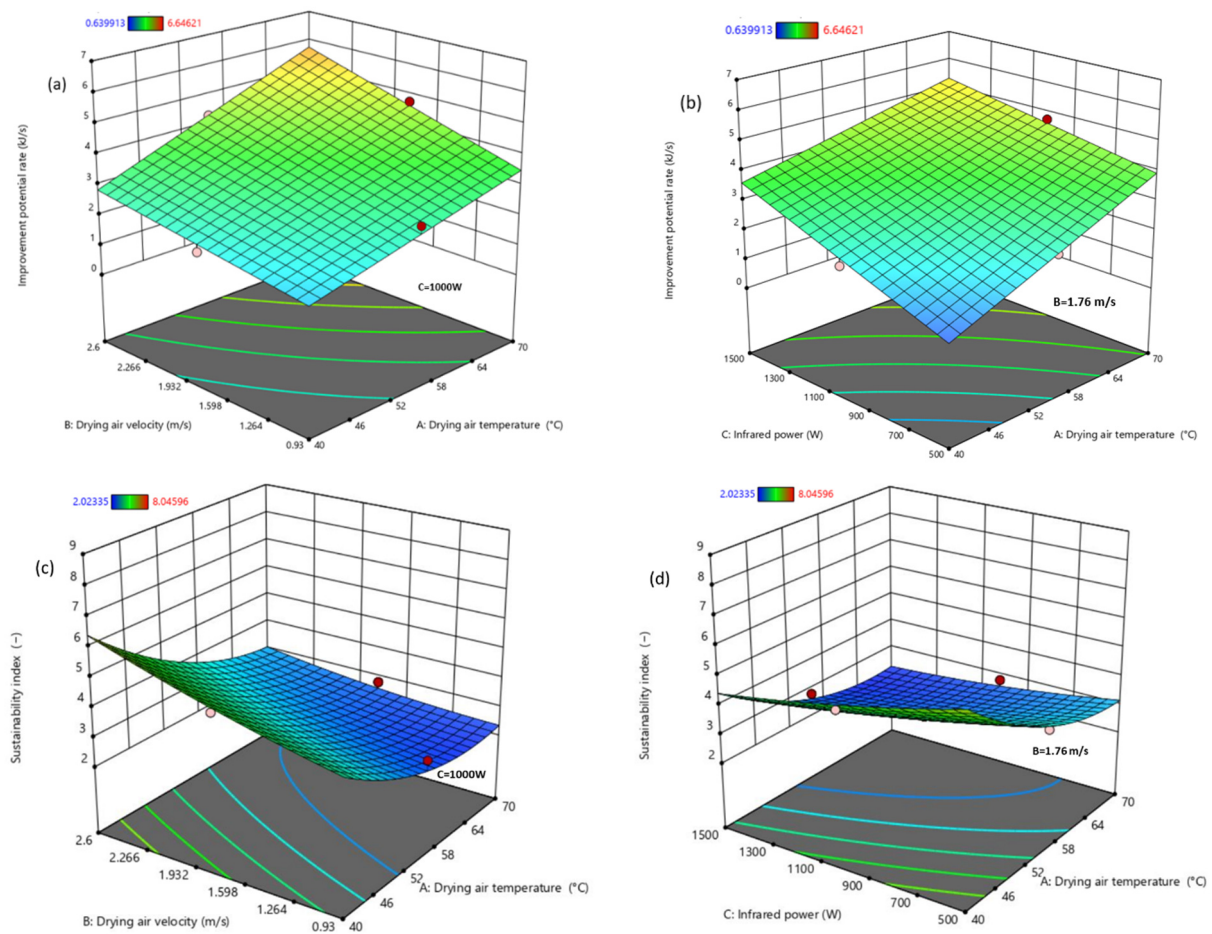

Figure 8. Response surface plot interaction between (**a**) air velocity and air temperature on $I\dot{P}$, (**b**) infrared power and air temperature on $I\dot{P}$, (**c**) air velocity and air temperature on SI, and (**d**) infrared power and air temperature on SI.

The effects of the air parameters and infrared power of the FBI dryer on the sustainability index of the drying chamber for drying terebinth fruit are demonstrated in Figure 8c,d. The value of SI enhanced with air velocity. It decreased with rising drying air temperature and infrared power. The sustainability index ranged from 2.023 to 8.045, while drying air temperature, air velocity, and infrared power varied in the range of 40–70 °C, 0.93–2.60 m/s, and 500–1500 W, respectively. The index in the study by Beigi [51] for drying kiwifruit slices in a convective tray dryer varied from 2.27 to 6.30. The minimum value of SI was 2.023 at a drying air temperature of 70 °C, drying air velocity of 0.93 m/s, and infrared power of 1500 W. The maximum value of this parameter was found to be 8.045 at 40 °C, 2.60 m/s, and 500 W, respectively (Figure 8c,d). Moreover, the effects of the independent variables on

the SI and exergetic efficiency of the drying chamber were the same. Thus, the exergetic efficiency of the drying process as an intensive operation of energy must be processed to diminish the environmental impact [51]. A great exergetic sustainability index depicts that a system has a significant effect on exergy savings and a low environmental impact because of exergy losses to the environment, which then has an effect on its economic value [58].

3.5. Multi-Objective Optimisation Process

A numerical procedure of optimisation was applied in the present study to obtain the optimised values of the input factors and relevant responses, along with the desired consequence. Moreover, the objective functions for this optimisation process were developed to minimise EU, EUR, exergy loss, and to maximise exergy efficiency, improvement potential rate, and sustainability index, which were also evaluated at the level of importance (3) to the variables. With respect to the results, the value of the desirability function after the optimisation process for this research was 0.670, as illustrated in Figure 9. This obtained result was almost above average values since the desirability function commonly ranged between 0 and 1, which showed the vicinity of the obtained output to the desired output [56,64]. Figure 9 shows that the optimised values of the input factors are air drying temperature at 40 °C, drying air velocity at 2.60 m/s, and infrared power at 633.65 W, and the obtained optimal values of related responses are 0.036 kJ/s for energy utilisation, 0.254 for energy utilisation ratio, 86.630% for exergy efficiency, 0.029 kJ/s for exergy loss rate, 1.793 kJ/s for improvement potential rate, 7.366 for sustainability index, and a desirability function of 0.670 at the end of the optimisation process. Figure 10 shows that the desirability function values for drying air temperature, drying air velocity, and infrared power are in the range of the optimisation process; therefore, the value of the desirability function is exactly 1, while the values for EU, EUR, EX_{eff}, EX_{loss}, $\dot{IP}$, and SI are 0.881, 0.785, 0.787, 0.974, 0.192, and 0.887, respectively. Furthermore, it should be noted that the overall combined desirability for this optimisation process is 0.670 (Figure 10).
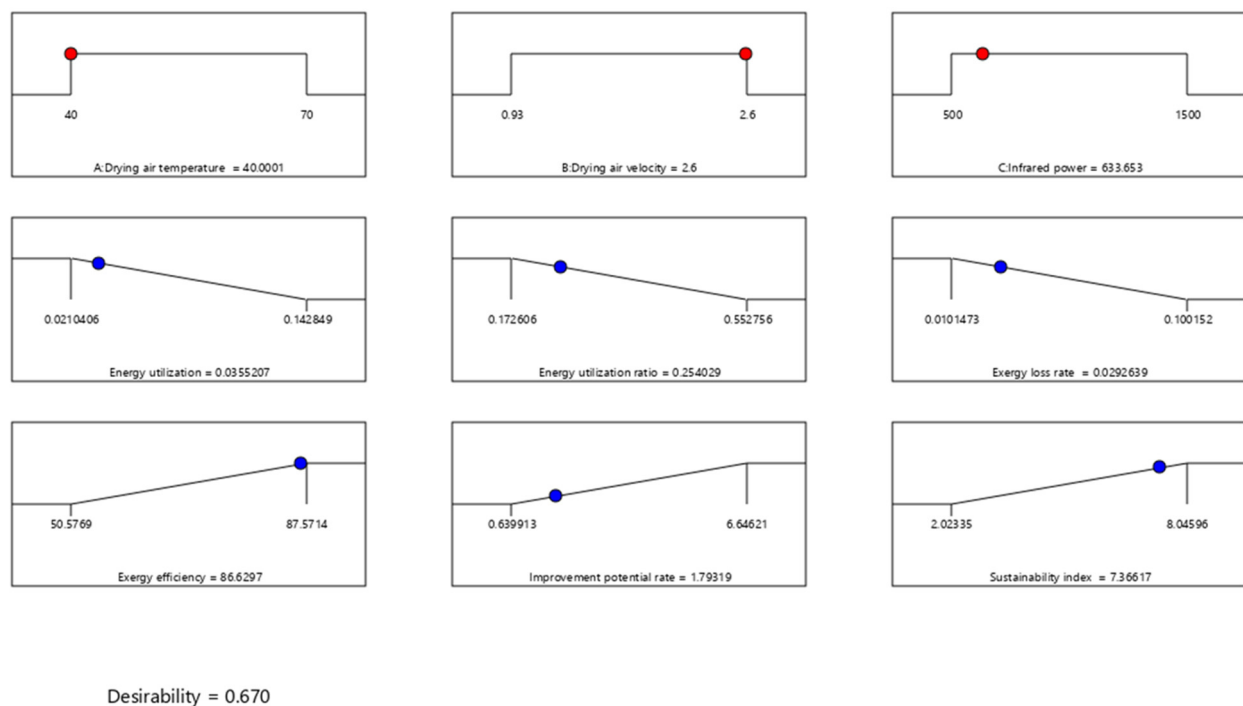

Figure 9. Ramp function graph of the desirability of the optimisation process drying conditions for the relevant responses using RSM.
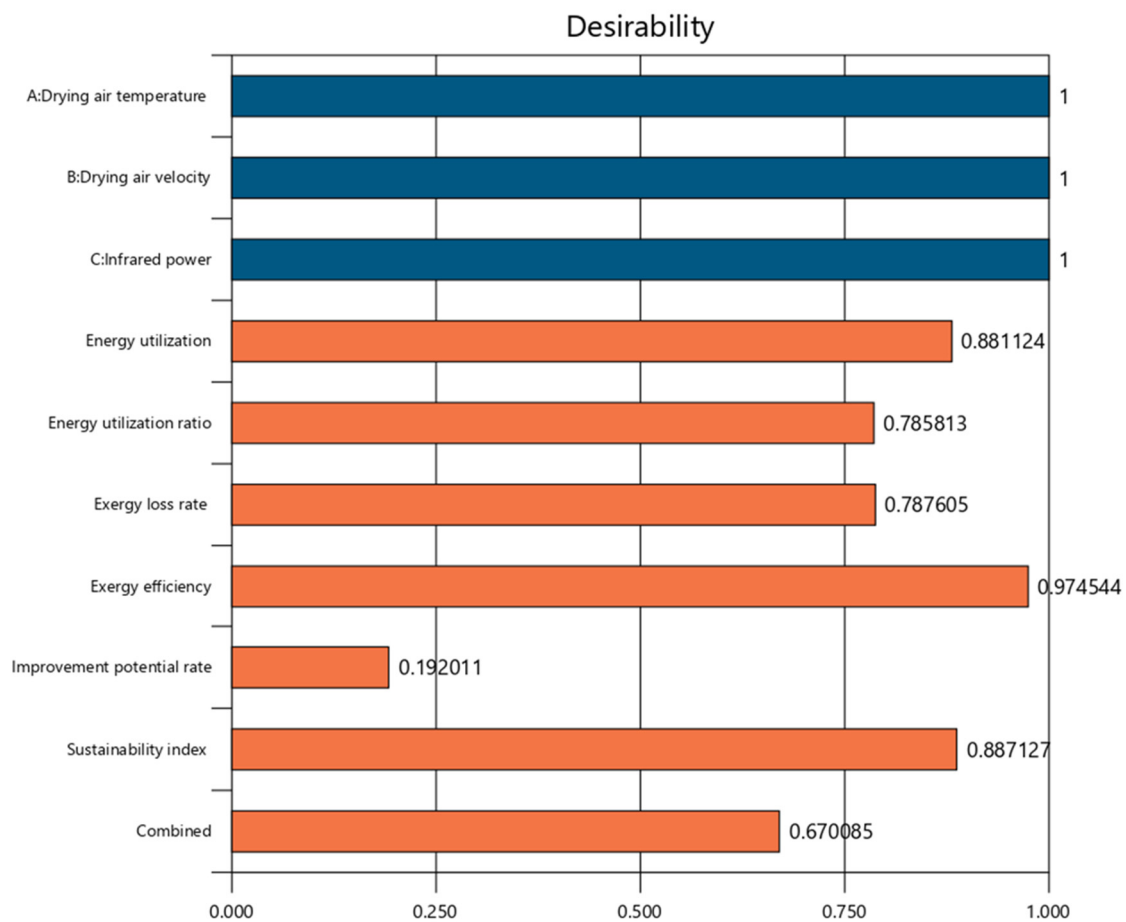
Figure 10. The values of individual desirability parameters for the independent and dependent variables and combined optimisation.

4. Conclusions

A procedure of CCD-RSM along with numerical modelling was utilised to investigate and assess the influence of various variables corresponding to the drying conditions of terebinth in a FBI dryer on the parameters of thermodynamics according to the objective functions. The optimisation process was performed to maximise exergy efficiency, improvement potential rate, and sustainability index, and to minimise energy utilisation, energy utilisation ratio, and sustainability index. The drying air temperature (40–70 °C), drying air velocity (0.93–2.60 m/s), and infrared power (500–1500 W) were in the range of the optimisation procedure. Variance analysis affirmed that the regression models of the RSM procedure had a great accuracy degree, showing that they could be applied to optimise the design of thermodynamic parameters and the drying operating conditions of terebinth. The results showed that energy utilisation, energy utilisation ratio, exergy efficiency, exergetic loss rate, improvement potential rate, and sustainability index were estimated to be 0.036 kJ/s, 0.254, 86.630%, 0.029 kJ/s, 1.793 kJ/s, and 7.366, respectively, while the optimal values for the drying conditions were specified as drying air temperature of 40 °C, drying air velocity of 2.60 m/s, and infrared power of 633.653 W. It is worth mentioning the developed statistical models of the multivariate RSM as an applied procedure could be helpful and trustworthy tools to estimate and optimise the thermodynamic performances during the drying of terebinth in the food industries. This is of utmost importance given the prominent need to minimise energy consumption in modern industrial processes.

Nomenclature

Notations

MC	moisture content (% dry weight)
T	temperature (°C)
P	atmospheric pressure (kPa)
V	air velocity (m/s)
A	area (m^2)
m	mass flow rate (kg/s)
c	specific heat (kJ/kg°C)
R	gas constant (8.3143 kJ/mol)
h	enthalpy (kJ/kg)
EU	energy utilisation (kJ/s)
EUR	energy utilisation ratio (kJ/s)
Q	heat transfer (kJ/s)
$\dot{En}$	energy rate (kJ/s)
EX	exergy rate (kJ/s)
ex	specific exergy (kJ/kg)
$\dot{IP}$	improvement potential rate (kJ/s)
SI	sustainability index
RSM	response surface method
D	total desirability function
Y	desirability function of each response in RSM
x	coded variable of model in RSM
n	number of responses
y	experimental value
$\bar{y}$	predicted value
HCI	hybrid convective infrared
$PRESS$	predicted sum of squares
$d.b.$	dry basis
SS	sum squares
CCD	central composite design
z	independent variables
U	total uncertainty
F	function of the independent variables
ADJ	adjusted
$PRED$	predicted
X	components of product (%)

Greek letters

ρ	density (kg/m^3)
δ	random error
ε	emissivity factor

ψ	exergy efficiency (%)
φ	relative humidity of air (%)
ω	humidity ratio (kg water/kg dry air)
σ	Stefan–Boltzmann constant ($\mathrm{W/m^2 \cdot K^4}$)
α	regression coefficient term of RSM's model
v	constant volume

Subscripts

0	ambient
a	air
IR	irradiation
fg	latent heat of vaporisation
vs	saturated vapour
loss	heat loss
ij	numerator
in	inlet
out	outlet
pred	predicted
te	terebinth
ex	exergy
dc	drying chamber
da	drying air
evp	evaporation
p	pressure
m	moisture
c	carbohydrate
pr	protein
f	fat
a	ash

References

1. Rababah, T.M.; Banat, F.; Rababah, A.; Ereifej, K.; Yang, W. Optimisation of extraction conditions of total phenolics, antioxidant activities, and anthocyanin of oregano, thyme, terebinth, and pomegranate. *J. Food Sci.* **2010**, *75*, 626–632.
2. Kaveh, M.; Abbaspour-Gilandeh, Y.; Taghinezhad, E.; Witrowa-Rajchert, D.; Nowacka, M. The Quality of Infrared Rotary Dried Terebinth (*Pistacia atlantica* L.)-optimisation and prediction approach using response surface methodology. *Molecules* **2021**, *26*, 1999.
3. Abbaspour-Gilandeh, Y.; Jahanbakhshi, A.; Kaveh, M. Prediction kinetic, energy and exergy of quince under hot air dryer using ANNs and ANFIS. *Food Sci. Nutr.* **2020**, *8*, 594–611.
4. Taheri-Garavand, A.; Karimi, F.; Karimi, M.; Lotfi, V.; Khoobbakht, G. Hybrid response surface methodology–artificial neural network optimisation of drying process of banana slices in a forced convective dryer. *Food Sci. Technol. Int.* **2018**, *24*, 277–291.
5. Golpour, I.; Amiri Chayjan, R.; Amiri Parian, J.; Khazaei, J. Prediction of paddy moisture content during thin layer drying using machine vision and artificial neural networks. *J. Agric. Sci. Technol.* **2015**, *17*, 287–298.
6. Golpour, I.; Nejad, M.Z.; Chayjan, R.A.; Nikbakht, A.M.; Guiné, R.P.F.; Dowlati, M. Investigating shrinkage and moisture diffusivity of melon seed in a microwave assisted thin layer fluidised bed dryer. *Food Meas.* **2017**, *11*, 1–11.
7. De Oliveira, R.M.; Andrade, K.S.; Prado, M.M.; Marques, L.G. Study on hybrid drying with infrared radiation of watermelon seeds (*Citrullus lanatus*). In *Defect and Diffusion Forum*; Trans Tech Publications Ltd.: Stafa-Zurich, Switzerland, 2020; Volume 399, pp. 173–182.
8. Majdi, H.; Esfahani, J.A.; Mohebbi, M. Optimisation of convective drying by response surface methodology. *Comput. Electron. Agric.* **2019**, *156*, 574–584.
9. Okunola, A.; Adekanye, T.; Idahosa, E. Energy and exergy analyses of okra drying process in a forced convection cabinet dryer. *Res. Agric. Eng.* **2021**, *67*, 8–16.
10. EL-Mesery, H.S.; Abomohra, A.E.F.; Kang, C.U.; Cheon, J.K.; Basak, B.; Jeon, B.H. Evaluation of infrared radiation combined with hot air convection for energy-efficient drying of biomass. *Energies* **2019**, *12*, 2818.
11. Özdemir, M.B.; Aktaş, M.; Şevik, S.; Khanlari, A. Modeling of a convective-infrared kiwifruit drying process. *Int. J. Hydrogen Energy* **2017**, *42*, 18005–18013.
12. Golpour, I.; Guiné, R.P.; Poncet, S.; Golpour, H.; Amiri Chayjan, R.; Amiri Parian, J. Evaluating the heat and mass transfer effective coefficients during the convective drying process of paddy (*Oryza sativa* L.). *J. Food Process. Eng.* **2021**, *44*, e13771.
13. Honarvar, B.; Mowla, D.; Safekordi, A.A. Experimental and theoretical investigation of drying of green peas in a fluidised bed dryer of inert particles assisted by infrared heat source. *Iran. J. Chem. Chem. Eng.* **2013**, *32*, 83–94.

14. Abbaspour-Gilandeh, Y.; Kaveh, M.; Fatemi, H.; Hernández-Hernández, J.L.; Fuentes-Penna, A.; Hernández-Hernández, M. Evaluation of the changes in thermal, qualitative, and antioxidant properties of terebinth (*Pistacia atlantica*) fruit under different drying methods. *Agronomy* **2020**, *10*, 1378.

15. Rashid, M.T.; Ma, H.; Jatoi, M.A.; Wali, A.; El-Mesery, H.S.; Ali, Z.; Sarpong, F. Effect of infrared drying with multifrequency ultrasound pretreatments on the stability of phytochemical properties, antioxidant potential, and textural quality of dried sweet potatoes. *J. Food Biochem.* **2019**, *43*, e12809.

16. Ghasemi, A.; Chayjan, R.A. Optimisation of pelleting and infrared-convection drying processes of food and agricultural waste using response surface methodology (RSM). *Waste Biomass Valoris.* **2019**, *10*, 1711–1729.

17. Taghinezhad, E.; Kaveh, M.; Szumny, A. Optimisation and prediction of the drying and quality of turnip slices by convective-infrared dryer under various pretreatments by RSM and ANFIS methods. *Foods* **2021**, *10*, 284.

18. Kocabiyik, H.; Yilmaz, N.; Tuncel, N.B.; Sumer, S.K.; Buyukcan, M.B. Drying, Energy, and Some Physical and Nutritional Quality Properties of Tomatoes Dried with Short-Infrared Radiation. *Food Bioprocess Technol.* **2015**, *8*, 516–525.

19. Aghbashlo, M. Exergetic simulation of a combined infrared-convective drying process. *Heat Mass Transf.* **2016**, *52*, 829–844.

20. Mugi, V.R.; Chandramohan, V.P. Energy and exergy analysis of forced and natural convection indirect solar dryers: Estimation of exergy inflow, outflow, losses, exergy efficiencies and sustainability indicators from drying experiments. *J. Clean. Prod.* **2021**, *282*, 124421.

21. Darvishi, H.; Zarein, M.; Farhudi, Z. Energetic and exergetic performance analysis and modeling of drying kinetics of kiwi slices. *J. Food Sci. Technol.* **2016**, *53*, 2317–2333.

22. Golpour, I.; Kaveh, M.; Chayjan, R.A.; Guiné, R.P.F. Energetic and exergetic analysis of a convective drier: A case study of potato drying process. *Open Agric.* **2020**, *5*, 563–572.

23. Li, C.; Li, B.; Huang, J.; Li, C. Energy and exergy analyses of a combined infrared radiation-counterflow circulation (ircc) corn dryer. *Appl. Sci.* **2020**, *10*, 6289.

24. Prommas, R.; Rattanadecho, P.; Cholaseuk, D. Energy and exergy analyses in drying process of porous media using hot air. *Int. Commun. Heat Mass Transf.* **2010**, *37*, 372–378.

25. Azadbakht, M.; Torshizi, M.V.; Ziaratban, A.; Aghili, H. Energy and exergy analyses during eggplant drying in a fluidised bed dryer. *Agric. Eng. Int. CIGR J.* **2017**, *19*, 177–182.

26. Darvishi, H.; Zarein, M.; Minaei, S.; Khafajeh, H. Exergy and energy analysis, drying kinetics and mathematical modeling of white mulberry drying process. *Int. J. Food Eng.* **2014**, *10*, 269–280.

27. Kaveh, M.; Chayjan, R.A.; Golpour, I.; Poncet, S.; Seirafi, F.; Khezri, B. Evaluation of exergy performance and onion drying properties in a multi-stage semi-industrial continuous dryer: Artificial neural networks (ANNs) and ANFIS models. *Food Bioprod. Process.* **2021**, *127*, 58–76.

28. Dolgun, G.K.; Aktaş, M.; Dolgun, E.C. Infrared convective drying of walnut with energy-exergy perspective. *J. Food Eng.* **2021**, *306*, 110638.

29. Afzali, F.; Darvishi, H.; Behroozi-Khazaei, N. Optimising exergetic performance of a continuous conveyor infrared-hot air dryer with air recycling system. *Appl. Therm. Eng.* **2019**, *154*, 358–367.

30. Sadeghi, E.; Haghighi Asl, A.; Movagharnejad, K. Optimisation and quality evaluation of infrared-dried kiwifruit slices. *Food Sci. Nutr.* **2020**, *8*, 720–734.

31. Benhamza, A.; Boubekri, A.; Atia, A.; El Ferouali, H.; Hadibi, T.; Arıcı, M.; Abdenouri, N. Multi-objective design optimisation of solar air heater for food drying based on energy, exergy and improvement potential. *Renew. Energy* **2021**, *169*, 1190–1209.

32. Icier, F.; Ozmen, D.; Cevik, M.; Cokgezme, O.F. Drying of licorice root by novel radiative methods. *J. Food Process. Preserv.* **2021**, *45*, e15214.

33. Icier, F.; Colak, N.; Erbay, Z.; Kuzgunkaya, E.H.; Hepbasli, A. A comparative study on exergetic performance assessment for drying of broccoli florets in three different drying systems. *Dry. Technol.* **2010**, *28*, 193–204.

34. Aghbashlo, M.; Kianmehr, M.H.; Arabhosseini, A. Performance analysis of drying of carrot slices in a semi-industrial continuous band dryer. *J. Food Eng.* **2009**, *91*, 99–108.

35. Akpinar, E.K.; Midilli, A.; Bicer, Y. Energy and exergy of potato drying process via cyclone type dryer. *Energy Convers. Manag.* **2005**, *46*, 2530–2552.

36. Choi, Y.; Okos, M.R. Effects of temperature and composition on the thermal properties of foods. In *Transport Phenomena*; Elsevier Applied Science Publishers: Basel, Switzerland, 1986.

37. Wepfer, W.J.; Gaggioli, R.A.; Obert, E.F. Proper evaluation of available energy for HVAC. *Ashrae Trans.* **1979**, *85*, 214–230.

38. Parhizi, Z.; Karami, H.; Golpour, I.; Kaveh, H.; Szymanek, M.; Blanco-Marigorta, A.M.; Marcos, J.D.; Khalife, E.; Skowron, S.; Othman, N.A.; et al. Modeling and optimisation of energy and exergy parameters of a hybrid-solar dryer for basil leaf drying using RSM. *Sustainability* **2022**, *14*, 8839.

39. Aghbashlo, M. A proposed mathematical model for exergy analysis of an infrared (IR) drying process. *Int. J. Exergy* **2015**, *18*, 480–500.

40. Beigi, M.; Tohidi, M.; Torki-Harchegani, M. Exergetic analysis of deep-bed drying of rough rice in a convective dryer. *Energy* **2017**, *140*, 374–382.

41. Brooker, D.B. Mathematical model of the psychrometric chart. *Trans. ASAE* **1967**, *10*, 558–560.

42. Islam, M.A.; Mondal, M.H.T.; Akhtaruzzaman, M.; Sheikh, M.A.M.; Islam, M.M.; Haque, M.A.; Sarker, M.S.H. Energy, exergy, and milling performance of parboiled paddy: An industrial LSU dryer. *Dry. Technol.* **2021**, *40*, 2058–2072. [CrossRef]

43. Hammond, G.P.; Stapleton, A.J. Exergy analysis of the United Kingdom energy system. *Proc. Inst. Mech. Eng. Part A J. Power Energy* **2001**, *215*, 141–162.

44. Holman, J.P. *Experimental Methods for Engineers*, 8th ed.; McGraw-Hill: New York, NY, USA, 2012.

45. Soltani, A.; Azzouz, S.; Romdhana, H.; Goujot, D. Multi-response optimisation of drying process parameters for Laurus Nobilis. *J. Appl. Res. Medic. Arom. Plant* **2021**, *22*, 100302.

46. Aghilinategh, N.; Rafiee, S.; Hosseinpour, S.; Omid, M.; Mohtasebi, S.S. Optimisation of intermittent microwave–convective drying using response surface methodology. *Food Sci. Nutr.* **2015**, *3*, 331–341.

47. Aneke, N.A.G.; Mbah, G.O.; Edeani, N.J. Response surface methodology for optimisation of hot air drying of water yam slices. *Int. J. Sci. Res. Public* **2018**, *8*, 248–259.

48. Gorji, T.B.; Ranjbar, A.A. Thermal and exergy optimisation of a nanofluid-based direct absorption solar collector. *Renew Energy* **2017**, *106*, 274–287.

49. Yogendrasasidhar, D.; Setty, P.Y. Drying kinetics, exergy and energy analyses of kodo millet grains and fenugreek seeds using wall heated fluidised bed dryer. *Energy* **2018**, *151*, 799–811.

50. Motevali, A.; Minaei, S. Effects of microwave pretreatment on the energy and exergy utilisation in thin-layer drying of sour pomegranate arils. *Chem. Ind. Chem. Eng. Q.* **2012**, *18*, 63–72.

51. Beigi, M. Moisture removal behavior and thermodynamic analysis of kiwifruit slices in convective tray dryer. *Lat. Am. Appl. Res.* **2022**, *52*, 119–126.

52. Corzo, O.; Bracho, N.; Vásquez, A.; Pereira, A. Energy and exergy analyses of thin layer drying of coroba slices. *J. Food Eng.* **2008**, *86*, 151–161.

53. Das, S.; Kashyap, D.; Bora, B.J.; Kalita, P.; Kulkarni, V. Thermo-economic optimisation of a biogas-diesel dual fuel engine as remote power generating unit using response surface methodology. *Therm. Sci. Eng. Progress.* **2021**, *24*, 100935.

54. Gupta, G.K.; Mondal, M.K. Bio-energy generation from sagwan sawdust via pyrolysis: Product distributions, characterisations and optimisation using response surface methodology. *Energy* **2019**, *170*, 423–437.

55. Nizamuddin, S.; Mubarak, N.M.; Tiripathi, M.; Jayakumar, N.S.; Sahu, J.N.; Ganesan, P. Chemical, dielectric and structural characterisation of optimised hydrochar produced from hydrothermal carbonisation of palm shell. *Fuel* **2016**, *163*, 88–97.

56. Obajemihi, O.I.; Olaoye, J.O.; Cheng, J.H.; Ojediran, J.O.; Sun, D.W. Optimisation of process conditions for moisture ratio and effective moisture diffusivity of tomato during convective hot-air drying using response surface methodology. *J. Food Process. Preserv.* **2021**, *45*, e15287.

57. Uzoma, S.; Nwakuba, N.; Anyaoha, K. Response surface optimisation of convective air drying process in a hybrid PV/T solar dryer. *Turk. J. Agric. Eng. Res.* **2020**, *1*, 111–130.

58. Alhanif, M.; Kumoro, A.C.; Wardhani, D.H. Mass transfer, energy utilisation, physical and nutritional properties evaluations during drying of papaya (*Carica papaya* L.) seeds at low to moderate temperatures. *Arab. J. Sci. Eng.* **2021**, *47*, 6245–6267. [CrossRef]

59. Mehran, M.; Masoum, S.; Memarzadeh, M. Microencapsulation of Mentha spicata essential oil by spray drying: Optimisation, characterisation, release kinetics of essential oil from microcapsules in food models. *June Ind. Crops Prod.* **2020**, *154*, 112694.

60. Myers, R.H.; Montgomery, D.C.; Anderson-Cook, C.M. *Response Surface Methodology: Process and Product Optimisation, Using Designed Experiments*; John Wiley & Sons: Hoboken, NJ, USA, 2016.

61. Stat-Ease, I. *Design Expert Software*; Educational Version 7.0.3; Wiley Publishing: New York, NY, USA, 2020.

62. Chakraborty, R.; Mukhopadhyay, P.; Bera, M.; Suman, S. Infrared-assisted freeze drying of tiger prawn: Parameter optimisation and quality assessment. *Dry. Technol.* **2011**, *29*, 508–519.

63. Aghbashlo, M.; Mobli, H.; Madadlou, A.; Rafiee, S. Influence of spray dryer parameters on exergetic performance of microencapsulation process. *Int. J. Exergy* **2012**, *10*, 267–289.

64. Rahmawati, L.; Saputra, D.; Sahim, K.; Priyanto, G. Optimisation of infrared drying condition for whole duku fruit using response surface methodology. *Potravin. Slovak J. Food Sci.* **2019**, *13*, 462–469.